I&EC research
Industrial & Engineering Chemistry Research

pubs.acs.org/IECR
Article

Properties and Intermolecular Forces of Ionic Liquid Mixtures: The Archetypical Case of [EMIM][BF_4] + [EMIM][$EtSO_4$]

Ylenia F. Rodríguez, Santiago Aparicio,* and Jose L. Trenzado*

Cite This: *Ind. Eng. Chem. Res.* 2025, 64, 1774−1791

ABSTRACT: The properties and nanostructure of the Double Salt−Ionic Liquid formed by the combination of [1-ethyl-3-methylimidazolium][BF_4] and [1-ethyl-3-methylimidazolium][$EtSO_4$] in the whole composition range are studied by a combined experimental and molecular simulation approach. The measured physicochemical properties were analyzed in terms of deviations of ideality and its relationships with intermolecular forces. Quantum chemistry calculations of model clusters were carried out to infer nanoscopic aggregations, considering several mechanisms of interactions. Classical molecular dynamics simulations were carried out as a function of mixture composition, pressure, and temperature, allowing one to characterize structural, dynamic, and energetic properties of the considered mixed ionic liquids. The possible mechanisms of interaction of the involved molecules with biological targets, proteins, and model cell membranes were also computationally studied to infer molecular level roots of toxicological effects of mixtures of ionic liquids. This multiapproach−multiscale study provides for the first time a global characterization of mixtures of ionic liquids.

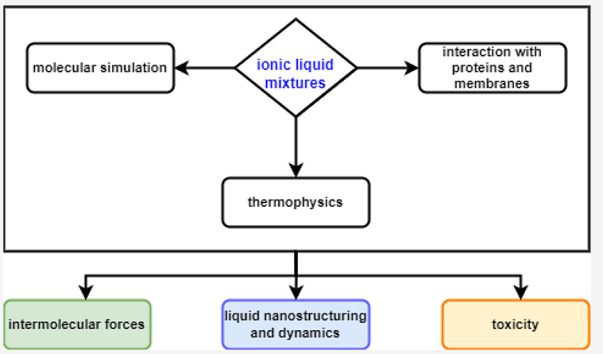

1. INTRODUCTION

Ionic liquids (ILs) have received special attention in recent decades, although they have been studied since the last century. The history of ILs started in 1914 when Walden prepared the first ionic liquid, ethylammonium nitrate (EAN),[1] which evolved when 40 years later, Hurley and Wier reported the second generation of ionic liquids by mixing alkylpyridinium chlorides with $AlCl_3$. Unfortunately, most of those initial ILs were not stable in the presence of humidity and it was not easy to regulate their acidity/basicity.[2] The evolution of IL research led to the last two decades, with the number of ILs published papers exponentially increasing from a few in 1996 to more than 5000 in 2016,[3] and the interest being maintained up to now with 6457 research documents containing the term ionic liquid indexed in the SCOPUS database. This maintained interest in IL properties, synthesis and technologies rises from all the proposed advantages ILs offer, in terms of their physicochemical properties, which indicate to be a future growing and continuing successful field.[4]

It should be mentioned that also certain criticism has been considered on the possible large-scale application of ILs, based on concerns about unsuitable physicochemical properties (e.g., large viscosity), toxicity, or poor biodegradation.[5−7] Nevertheless, many of these possible drawbacks may be avoided via the proper selection of suitable ions, leading to ILs among the plethora of possible compounds.

What makes Ionic liquids so particular is their exclusively composed ions structure, not like usual solvents composed of neutral molecules, and remaining in liquid state at room temperature. Combinations of cations and anions of different characteristics and sizes cause ionic liquids properties to vary in one direction or another, allowing adapting their properties to the needs required (*tailor-made solvents*). Physicochemical properties may be fine-tuned via regulation of the molecular structures of the involved ions, e.g. Dong et al. observed that the viscosity increases with increasing cation alkyl chain length (e.g., imidazolium and pyridinium)[4] Density is also another property strongly affected by ion characteristics, for example, it usually increases with anion molecular mass.[8] Their exceptional range of tunable properties is one of the key reasons behind the growing interest in ionic liquids, and the development and understanding of the structure−property relationship is fundamental to understanding IL behavior. The capacity to tune their properties made them a perfect tool, allowing the design of tailor-solvents for the required technologies and offering a replacement for traditional volatile organic compounds (VOCs).

There are multiple studies that broadly analyze the potential applications for ILs, including remarkable catalytic perform-

Received: July 31, 2024
Revised: October 16, 2024
Accepted: October 23, 2024
Published: January 10, 2025

https://doi.org/10.1021/acs.iecr.4c02839
Ind. Eng. Chem. Res. 2025, 64, 1774−1791

ance,[9] good behavior as gas adsorbents or extractant agents[10−12] and excellent lubricant properties.[13−15] In addition, researchers continue to explore the broad potential of ILs in new and unexplored fields. Khupse and Kumar studied ionic liquid utilization in electrochemical devices such as supercapacitors, lithium-ion batteries, or polymer-electrolyte fuel cells. Two main advantages of using ionic liquids include nonvolatility and prevention of electrolytes.[16] The concept of *IoNanofluids* was proposed by Nieto de Castro and co-workers; it represents a new class of heat transfer fluids where nanomaterials like particles, tubes, and rods are dispersed in ionic liquids. IoNanofluids are one of the most recent applications of complex systems of ionic liquids and nanomaterials, they could be used for heat transfer to catalysis, lubricants, or luminescent materials.[17] Due to the unique properties of ILs, their application in the pharmaceutical field has been extended in numerous processes, from drug synthesis to the development of new solubilization and dosage forms of active pharmaceutical ingredients (API-ILs), with research also being carried out at other stages of drug development and delivery. Research has shown that the proper selection of anion/cation combinations has a significant impact on the solubilization mechanism of poorly water-soluble APIs.[18]

The combination of more than two types of ions is known to possibly exhibit unexpected associations that yield nonideal properties. Double salt ionic liquids (DSILs) are thus defined as ionic liquids containing more than one cation or anion and presenting different physicochemical properties than their component single salts. Many properties of DSILs, such as solubility, are dependent on chemical associations between the ions, and altering the ionic ratios can induce different chemical interactions leading to new properties.[19] The combination of ions can induce preferential orientation of ionic species and noncovalent interaction. The advantage of using DSILs depends on a suitable anion−cation combination to accomplish more efficiently by designing task-specific IL mixtures. Although DSILs offer significant advantages over classical pure ILs, relevant studies are still scarce, and a systematic DSIL selection method is thus highly desirable.[20] Therefore, the aim of this work was to study the physicochemical properties, nanostructuring, and biological effects of DSILs formed by the combination of 1-ethyl-3-methylimidazolium cation coupled with bistriflimide and ethylsulfate ([EMIM][BF_4] and [EMIM][$EtSO_4$]), leading to IL binary mixtures containing a common cation (DSILs), as shown in Figure 1. All physicochemical properties were reported in the full composition range as a function of temperature. Microstructuring and characterization of intermolecular forces allow us to infer the mechanism of molecular interaction between [EMIM][BF_4] and [EMIM][$EtSO_4$] ILs and their binary constituent mixtures with $[EMIM]^+$ as a common cation. The selection of these ILs to be mixed was done considering that the available literature has shown minor deviations from ideality but the nanoscopic behavior of these systems has not been extensively studied, neither the evolution of excess and mixing properties nor in the changes in intermolecular forces upon mixing and the local composition effects. Likewise, the possible biological effects of the considered DSILs were in silico studied through the consideration of their interaction with target biomolecules as well as with model cell membranes. The main innovation of this work consists in the combination of thermophysical studies with molecular modeling, which can provide the necessary knowledge about the properties of the mixture considering a multiscale approach.[20]

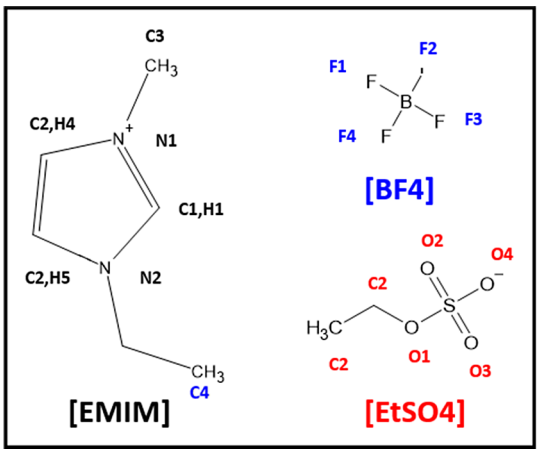

Figure 1. Ions forming ILs considered in this work as well as labeling for relevant atoms.

2. METHODS

2.1. Chemicals. The studied ionic liquids [EMIM][BF_4] and [EMIM][$EtSO_4$] used for the experimental study were supplied by a commercial provider (Sigma-Aldrich) and were used without additional purification, Table S1 (Supporting Information). Pure ILs were degassed by ultrasound and stored under suitable conditions. All the properties of pure ILs were measured as a function of temperature in the 283.15−313.15 K range, in 5 K steps at atmospheric pressure, and compared with literature (Table S2, Supporting Information), showing minor differences. The presence of relevant impurities was discarded, differences can be attributed to water content and different origins of the samples. The mixture samples (x [EMIM][BF_4]+ $(1 - x)$ [EMIM][$EtSO_4$], where x stands for mole fraction) were prepared in the full composition range by weighing (Mettler AE240 balance, ± 0.01 mg) to ±0.00004 estimated mole fraction uncertainty.

2.2. Apparatus and Procedures. Density (ρ) and kinematic viscosity (ν) were measured for x [EMIM][BF_4] + $(1 - x)$ [EMIM][$EtSO_4$] liquid mixtures, where x stands for mole fraction, in the full composition range, at atmospheric pressure and temperature in the 283.15−313.15 K range in 5 K steps. ρ was measured with a vibrating tube densimeter (Anton Paar DMA5000, uncertainty 1×10^{-4} g cm^{-3}), with Peltier control for the cell temperature (uncertainty 0.01 K). The thermal expansion coefficient, α_p, was calculated according to its thermodynamic definition:

$$\alpha_p = -\frac{1}{\rho}\left(\frac{\partial \rho}{\partial T}\right)_p = -\frac{1}{\rho}a \quad (1)$$

where a is the slope of the corresponding ρ vs temperature linear fit.

ν was measured using various Ubbelohde viscometers according to the required viscosity range, in an external circulating bath with a cell temperature measured with ±0.01 K uncertainty (CT-52, Schott Instruments) and an automatic control unit AVS350 (Schott, ViscoSystem) with ±0.01 s uncertainty. Dynamic viscosity (η) was calculated as in eq 2.

$$\eta = \nu\rho \quad (2)$$

The expanded uncertainties of the experimental properties (0.95 confidence level) are as follows: $Uc(T)$ = ± 0.01 K. $Uc(x)$ = ±

https://doi.org/10.1021/acs.iecr.4c02839
Ind. Eng. Chem. Res. 2025, 64, 1774−1791

0.00001. $Uc(\rho) = \pm 0.00001$ g cm^{-3}. $Uc(\nu) = \pm 0.01$ mm^2 s^{-1}; $Uc(\eta) = \pm 0.01$ mPa s.

The viscosity versus temperature evolution was described according to the Vogel−Fulcher−Taman (VFT) model:

$$\eta = \eta_0 \exp\left(\frac{B}{T - T_0}\right) \tag{3}$$

VFT fitting parameters were used for the calculation of Angell's strength (fragility measurement) parameter, D_f.

$$D_f = \frac{B}{T_0} \tag{4}$$

Experimental density data were considered for the calculation of excess molar volume, V^E:

$$V^E = \frac{\sum_{i=1}^{2} x_i M_i}{\rho} - \sum_{i=1}^{2} x_i \frac{M_i}{\rho_i} \tag{5}$$

where M_i is the molar mass of the component i, ρ_i and ρ the densities of the pure compound i and for the corresponding mixture, respectively. Likewise, the excess thermal expansion coefficient, α_p^E, was calculated as follows:

$$\alpha_p^E = \alpha_p - \sum_{i=1}^{2} \varphi_i \alpha_{p,i} \tag{6}$$

where α_p and $\alpha_{p,i}$ are the thermal expansion coefficients of the mixture and pure component i, respectively; φ_i stands for the volume fraction of component i, φ_i:

$$\varphi_i = \frac{x_i V_i^*}{\sum_{i=1}^{2} x_i V_i^*} \tag{7}$$

where x_i stands for the mole fraction of i component and V_i^* for the molar volume of pure i compound. For the case of viscosity, as the ideal state reference term cannot be defined and thus excess property could not be considered, the so-called mixing viscosity, $\Delta\eta$, was calculated:

$$\Delta\eta = \eta - \sum_{i=1}^{2} x_i \eta_i \tag{8}$$

Additionally, excess and mixing properties were fitted to an isothermal Redlich−Kister type polynomial equation as a function of mole fraction, x:

$$Y^E = x(1 - x) \sum_{i=0}^{n} A_i (1 - 2x)^i \tag{9}$$

Likewise, the partial molar volume $\overline{V}_i$ of each component i was calculated:

$$\overline{V}_i = V_m^E + V_i^* + (1 - x_i)\left(\frac{\partial V^E}{\partial x_i}\right)_{T,P} \tag{10}$$

where V_i^* stands for the molar volume of pure component i, with the partial derivative of the excess volume calculated from the corresponding Redlich−Kister coefficients. Excess partial molar volumes, $\overline{V}_i^E$, were defined as

$$\overline{V}_i^E = \overline{V}_i - V_i^* \tag{11}$$

The excess partial molar volumes at infinite dilution, $\overline{V}_i^{E,\infty}$ were calculated:

$$\overline{V}_i^{E,\infty} = \overline{V}_i^{\infty} - V_i^* \tag{12}$$

where the partial molar volume at infinite dilution, $\overline{V}_i^{\infty}$, is defined as the corresponding limiting value when $x_i \to 0$. All the relevant thermophysical properties and the corresponding fitting parameters are reported in Tables S3−S5 (Supporting Information).

Parameters for the modeling of excess volume according to the Prigogine−Flory−Patterson (PFP)[21] model are reported in Table S6 (Supporting Information).

2.3. Density Functional Theory Calculations. Intermolecular interactions between involved anions and cations were analyzed considering different ionic clusters (dimmers and tetramers), whose structures were optimized through density functional theory (DFT) calculations carried out with Dmol3[22] software. The main objective of DFT calculations is to analyze the nature of intermolecular forces in the considered IL mixtures, in particular, for the characteristics of hydrogen bonding. For that purpose, dimmers and higher aggregates were built, and their geometries were optimized through energy minimization. All the calculations were carried out at the GGA/PBE plus Grimme's D3[23] dispersion contribution theoretical level. The optimized geometries for the considered clusters were used for the calculation of the interaction energy, ΔE, as the difference between the energy of the corresponding cluster and the sum of the corresponding monomers. All the ΔE were corrected for the basis set superposition error (BSSE) using the counterpoise method.[24] Regarding the accuracy of calculated ΔE, it is estimated to be in the 8−13 kJ mol^{-1},[25] which is well beyond the large ΔE values for anion−cation interactions in ILs (roughly 1%).

The topological properties of the clusters were analyzed considering the quantum theory of atoms in molecule (Bader's QTAIM theory)[26] as in MultiWFN software,[27] considering electron density (ρ_e) and Laplacian of the electron density ($\nabla^2\rho_e$), of bond (BCPs, type (3,−1) in QTAIM) and Ring (RCPs, type (3,−1) in QTAIM) critical points. and electron localization function (ELF) using core−valence bifurcation index (CVB[28]) were also considered as well as Interaction Region Indicator (IRI) analysis.[27]

2.4. Classical Molecular Dynamics Simulations. Classical MD simulations were carried out using the MDynaMix v.5.2 program.[29] The force field parametrizations for the three types of ions considered in this work ($[EMIM]^+$,$[BF_4]^-$ and $[EtSO_4]^-$ (Table S7, Supporting Information) were obtained from SwissParam database (Merck Molecular Force Field[30]), except atomic charges which were computed from DFT calculations of ions using ChelpG method. Simulation boxes were built as indicated in Table S8 (Supporting Information) for covering the whole mixture composition range, as well as for different pressure and temperature conditions to analyze their effect on mixture properties. Initial cubic simulation boxes were prepared with the Packmol program.[31] All MD simulations were carried out according to a two-stage procedure: (i) NVT simulations at the considered conditions for 10 ns, followed by (ii) NPT simulations at the considered pressure and temperature conditions for 200 ns, which were used for the analysis of mixtures properties.

All MD simulations were performed by considering periodic boundary conditions along the three space directions. The equations of motion were solved considering the Tuckerman−Berne double-time step algorithm[32] with 1.0 and 0.1 fs for long and short-time steps. Electrostatic interactions were treated with

https://doi.org/10.1021/acs.iecr.4c02839
Ind. Eng. Chem. Res. 2025, 64, 1774−1791

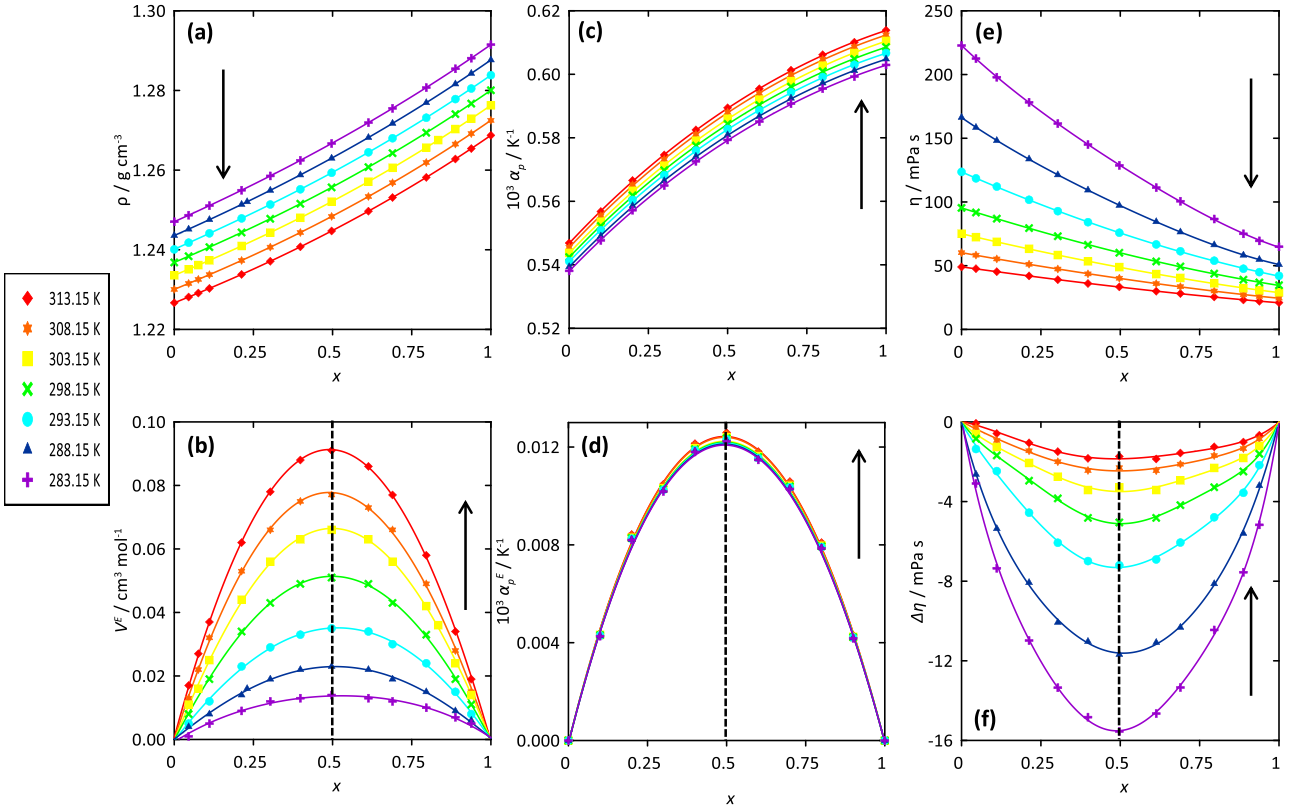

Figure 2. Experimental thermophysical properties for x [EMIM][BF4] + $(1 - x)$ [EMIM][EtSO4], where x stands for mole fraction, as a function of temperature. (a) Density (ρ), (b) excess molar volume (V^E), (c) isobaric thermal expansion coefficient (α_p), (d) excess isobaric thermal expansion coefficient (α_p^E), (e) dynamic viscosity (η), and (f) mixing viscosity ($\Delta\eta$). Black arrows indicate an increasing temperature for guiding purposes. Dashed lines in panels b,d and f show equimolar composition to show position of the maxima in the corresponding excess or mixing property.

the Ewald method[33] (15 Å for cutoff radius). Lennard−Jones potential was considered (15 Å cutoff distance) with Lorentz−Berthelot mixing rules for cross terms. Temperature and pressure were controlled with the Nose−Hoover method.[34] The visualization and analysis of MD trajectories were carried out with VMD[35] and TRAVIS.[36]

2.5. Coarse-Grained Classical Molecular Dynamics Simulations of Ionic Liquid−Lipid Bilayer Interactions. The possible biological negative effects of the considered IL mixture may be studied using the concept of adverse outcome pathways (AoPs), i.e. the sequence of events, from molecular to cellular to organ levels, which leads to a toxic effect of a substance on a living organism.[37] The series of complex processes leading to final toxicity is proposed to be initiated from a so-called molecular initiating event (MiE).[38] A particularly well-known MiE is the interaction of chemicals with plasma (cell) membranes.[39] For this purpose, the mechanism(s) of interaction of the considered IL mixtures with a model cell membrane, formed by a DPPC lipid bilayer, and the changes in the membrane properties in the presence of ILs in an aqueous solution were analyzed using Coarse Grained Molecular Dynamics (CG-MD) simulations. The reason to study the IL−lipid bilayers interactions using CG-MD simulations instead of All Atom simulations (as indicated in Section 2.4 for liquid phase properties) stands on the size of the considered systems (water + IL + lipid bilayer with a large number of atoms) as well as considering the time scale required to infer lipid bilayer changes; therefore, CG-MD provides a suitable solution to provide results at a reasonable computational cost.

CG-MD simulations were carried out considering IL mixtures in aqueous solutions at different concentrations (Table S9, Supporting Information). The beading of the ions, water, and DPPC molecules is explained in Figure S1 (Supporting Information). CG force field parametrization was done according to the Martini3 CG force field[40] (Figure S1, Supporting Information). The suitability of the Martini force field for describing ILs has been recently probed,[41] and thus, the CG-MD approach is a suitable option for describing the behavior of the considered IL mixtures at model plasma membranes. Water solutions in contact with DPPC bilayer for 17−20 wt % content of IL mixtures were considered, with these IL mixtures corresponding to x [EMIM][BF_4] + $(1 - x)$ [EMIM][$EtSO_4$] with 0, 0.25, 0.50, 0.75, and 1.00 mole fraction.

CG-MD simulations were carried out with the MESOCITE/Materials Studio software. Simulations were carried out in a three stages procedure: (i) energy minimization through geometry optimization using the conjugated gradient method, (ii) 1 ns NVT simulations at 318 K with the Velocity Scale method for temperature control, and (iii) 500 ns NPT simulations at 318 K (Nose thermostat) and 1 bar (Berendsen barostat); 1.0 ps was used for coupling constants of the thermostat and barostat along all the simulations, and a 20 fs time step was used for all the simulations. Electrostatics (i.e., Coulombic interactions) were handled with the Ewald method and van der Waals with a group (bead) based cutoff method, 15.0 Å cutoffs.

2.6. Interaction of the Ionic Liquid with Model Biomolecules. Additional studies on the possible negative biological effects of the considered IL mixtures were in silico

https://doi.org/10.1021/acs.iecr.4c02839
Ind. Eng. Chem. Res. 2025, 64, 1774−1791

conducted through the analysis of the interaction of the involved IL molecules with target biomolecules. For this purpose, four biomolecules were selected: 1BNA (B-DNA dodecamer), 1AO6 (human serum albumin), 1QZR (ATPase region of *Saccharomyces cerevisiae* topoisomerase), and (cyclooxygenase-2 (prostaglandin synthase-2). Docking calculations for IL molecular clusters corresponding to ten different arrangements inferred from results in Section 2.3 on the four selected biomolecules were carried out. The biomolecule structures were obtained from the Protein Databank and prepared using Autodock Tools with docking regions containing the whole biomolecules (i.e., not−guided docking). Docking studies were carried out using Autodock Vina[42] with the obtained docked structures being ranked through the corresponding affinities (scores).

3. RESULTS AND DISCUSSION

3.1. Macroscopic and Thermodynamic Characterization. Density and kinematic viscosity values for pure ILs [EMIM][BF4] and [EMIM][EtSO4] and their binary mixtures in the full composition range have been experimentally measured in the 283.15−313.15 K range. These properties, as well as the derived ones, are reported in Figure 2. For the analysis of density data reported in Figure 2a, it should be initially remarked that although both pure ILs are largely dense fluids, [EMIM][BF4] is denser than [EMIM][EtSO4], 3.5% denser on average in the considered temperature range. The usual trend on the density for ILs showing a common cation (in this case [EMIM]) is the increase of density with the molar mass of the anion,[8] but an opposite behavior is inferred for [BF4] and [EtSO4], in which the lightest anion ([BF4], M = 86.80 g mol^{-1}) is denser than the heaviest one ([EtSO4], M = 125.12 g mol^{-1}), and thus, further effects need to be considered. Considering the relevance of anion−cation interactions on the ILs properties, the structures of [EMIM][BF4] 1:1 and [EMIM][EtSO4] 1:1 dimer clusters were optimized using DFT and their properties, analyzed to infer relationships with fluids' density. The volume of the optimized dimers, in which cations and anions are hydrogen-bonded, was calculated and from that, an estimation of the density was inferred via the ratio of this volume and the dimer molar mass of the cluster, which, although neglecting additional effects present in the liquid phase, provide a rough estimation of fluids density. The inferred densities are 1.12 and 1.08 g cm^{-3}, for [EMIM][BF4] and [EMIM][EtSO4], respectively, although being roughly 13% lower than the experimental values reported in Figure 2a, confirm that [BF4]−containing IL is roughly 3.5% denser than IL containing [EtSO4], and it shows the pivotal role of the nature of the developed [EMIM]−anion hydrogen-bonded cluster on the properties of the bulk fluid. The evolution of density with mixture composition as reported in Figure 2a is slightly nonlinear, which leads to positive V^E, i.e. expansion upon mixing, although V^E are not too large and decrease upon heating, thus indicating low deviations from ideality. The low values for excess properties have been previously reported for different types of ILs.[43−45] Chakraborty et al.[45] proposed that [alkylimidazolium]−based IL mixtures with a common cation usually showed positive V^E because of the excess molar volume for imidazolium-based IL−IL mixtures may be linked to the free volume created by the alkyl chain, although negative V^E has also been reported for [alkylimidazolium]−containing mixtures.[42] The results obtained in this work for [EMIM][BF4]−[EMIM]-[EtSO4] mixtures may be compared with those from Navia et al.[43] for [1-butyl-3-methylimidazolium][BF4] ([BMIM][BF4]) - [1-butyl-3-methylimidazolium][methylsulfate] ([BMIM]-[MeSO4]). In the case of [BMIM][BF4]−[BMIM][MeSO4] with a minima for V^E of roughly -0.06 cm^3 mol^{-1} at equimolar mixture composition and 303 K in contrast with a maxima of 0.065 cm^3 mol^{-1} for [EMIM][BF4]−[EMIM][EtSO4]. This behavior confirms the role of the size of cation alkyl chains on the development of free space to fit cations; in the case of [BMIM] larger free space is produced than for [EMIM], which allows the proper fitting of the smaller [MeSO4] anions in comparison with the larger [EtSO4] ones. Nevertheless, in both cases deviations from ideality are very low (positive or negative), thus pointing to an effect of free space rearrangement upon mixing with negligible disruption in the established intermolecular forces.

The calculated α_p values are reported in Figure 2c. Pure [EMIM][BF4] is more compressible than [EMIM][EtSO4], in agreement with the literature.[46,47] The α_p evolution with mixture composition shows a nonlinear behavior, which leads (Figure 2d) to positive α_p^E (i.e., more compressible fluids upon mixing) with maxima at equimolar composition and almost negligible effect of the temperature. Nevertheless, the reported positive α_p^E values are very low (roughly 0.012 × 10^{-3} K^{-1}), thus leading to almost ideal mixtures considering this property and pointing again to very minor restructuring effects rising from the available free space as the main effect upon mixing in terms of compressibility.

The dynamic properties of the considered IL mixtures were macroscopically analyzed through the dynamic viscosity (Figure 2e). First, it should be remarked that pure [EMIM][EtSO4] is roughly three times more viscous than [EMIM][BF4]. The viscosity evolution with temperature for both pure ILs as well as for the studied mixtures cannot be described according to an Arrhenius model, and thus VFT fitting was considered for all the systems. The calculated VFT parameters allowed us to infer the D_f (fragility) parameter. The D_f values for pure ILs are 3.19 and 3.04 for [EMIM][EtSO4] and [EMIM][BF4], respectively, and thus, although [EMIM][EtSO4] is more fragile, both fluids may be considered fragile ones. In spite of the small differences in the pure fluids' fragility, the large differences between the viscosities of both ILs lead to a nonlinear evolution of viscosity upon mixing and, thus, to negative non-negligible $\Delta\eta$ (Figure 2f). The negative $\Delta\eta$ are usually assigned to factors such as fewer surfaces available for friction,[48] or mainly to the weakening of intermolecular forces between molecules.[49] The case of negative non-negligible $\Delta\eta$ for [EMIM][BF4]−[EMIM][EtSO4] does not seem to be produced from large variations of intermolecular forces, as discarded from the very low excess properties reported in Figure 2b,d. Although $\Delta\eta$ is not an excess property, in the thermodynamic sense (ideal state is not possible to define), the decrease in viscosity upon mixing should rely on the rearrangement of molecular clusters upon mixing. It has been reported that large negative $\Delta\eta$ is obtained when mixing ILs with dissimilar structures,[50] which is confirmed for [BF4] and [EtSO4] anions. This is also inferred from the large differences between the viscosities of pure ILs ([EtSO4] > [BF4]), which may be also related to the differences among the intermolecular forces in each pure IL. This effect is confirmed by literature results showing the large cation effect,[49] for [EMIM][NTf2]−[EMIM][EtSO4] showed very small $\Delta\eta$ (<4 mPa s) in contrast with [EMIM][NTf2]−[BMIM][EtSO4] ($\Delta\eta$ maximum of 60 mPa s). In the case of [EMIM][BF4]−[EMIM][EtSO4] the anion type effect rises from the type of anion−cation

https://doi.org/10.1021/acs.iecr.4c02839
Ind. Eng. Chem. Res. 2025, 64, 1774−1791

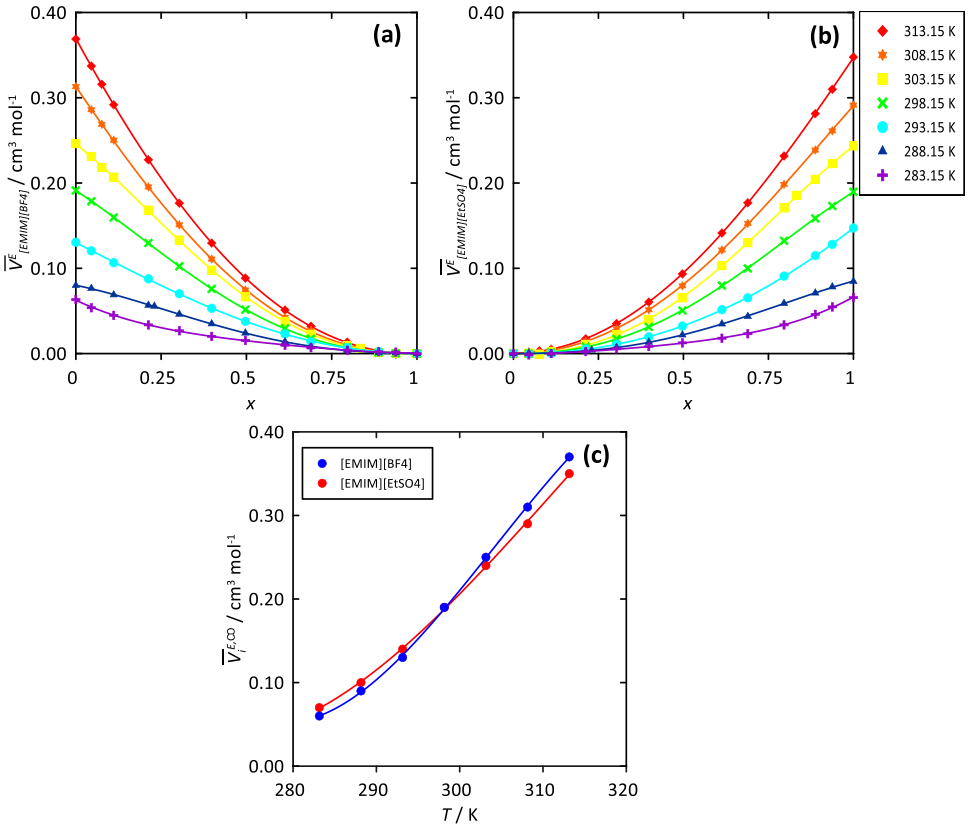

Figure 3. (a, b) Excess partial molar volume of component i, $\overline{V}_i^{E}$, and (c) values at infinite dilution, $\overline{V}_i^{E,\infty}$, for x [EMIM][BF4] + $(1 - x)$ [EMIM][EtSO4], where stands for mole fraction, as a function of temperature. Black arrows indicate increasing temperature for guiding purposes. Panels a and b show the results for [EMIM][BF_4] and [EMIM][TFSI], respectively.

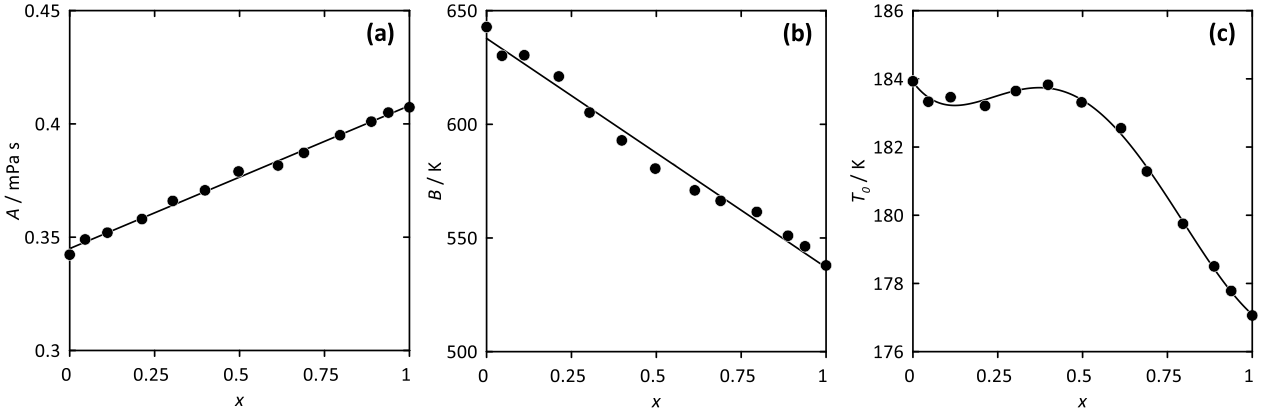

Figure 4. Fitting parameters of VFT equation for experimental dynamic viscosity of x [EMIM][BF4] + $(1 - x)$ [EMIM][EtSO4], where stands for mole fraction, in the 283.15−313.15 K temperature range.

intermolecular forces (hydrogen bonding), being C(H)−F (for [BF4]) in contrast with C(H)−O (for [EtSO4]), and thus, although the effect of anion on viscosity is less remarkable than the cation one, it is the main reason for the negative $\Delta\eta$. Nevertheless, large changes in intermolecular forces are not produced but the differences in those upon mixing should be noted.

Further analysis of the mixed IL structuring is carried out by considering the excess partial molar volumes reported in Figure 3a,b for each IL mixture component. The reported $\overline{V}_i^{E}$, and the values at infinite dilution, $\overline{V}_i^{E,\infty}$, Figure 3c, show symmetric behavior for both mixture components, i.e., minor disruption of each IL structuring upon mixing, leading to low positive $\overline{V}_i^{E}$ in agreement with the low V^E values (Figure 2b). The low and positive $\overline{V}_i^{E,\infty}$ values indicate a proper fitting of each type of IL into the structure of the second one with almost negligible disruption. These results confirm that the mixing is produced by the fitting of each IL into the other one structuring with negligible disruptions of intermolecular forces, thus resulting in small excess properties.

The behavior of $\overline{V}_i^{E}$ is very symmetric for both components, with similar positive values in the whole composition range and increasing with temperature. These values of the excess partial molar volumes confirm the strength of intermolecular forces. Likewise, the large values of $\overline{V}_i^{E,\infty}$ show the disrupting effect of

https://doi.org/10.1021/acs.iecr.4c02839
Ind. Eng. Chem. Res. 2025, 64, 1774−1791

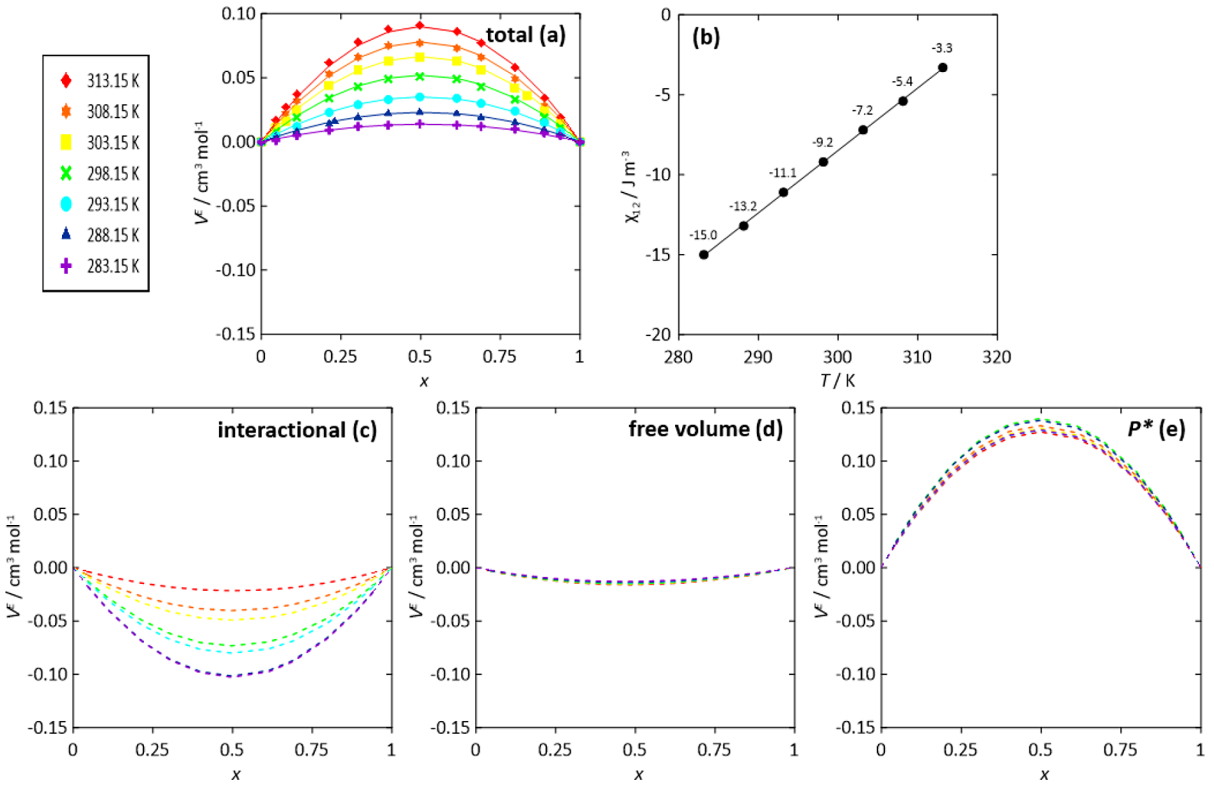

Figure 5. (a) Comparison of experimental, symbols, and PFP (lines) excess molar volume, V^E, with the PFP interaction coefficient, χ_{12}, reported in (b) x [EMIM][BF4] + $(1 - x)$ [EMIM][EtSO4], where stands for mole fraction, as a function of temperature. Results in panels c-e show interactional, free volume, and P^* PFP contributions to the total V^E.

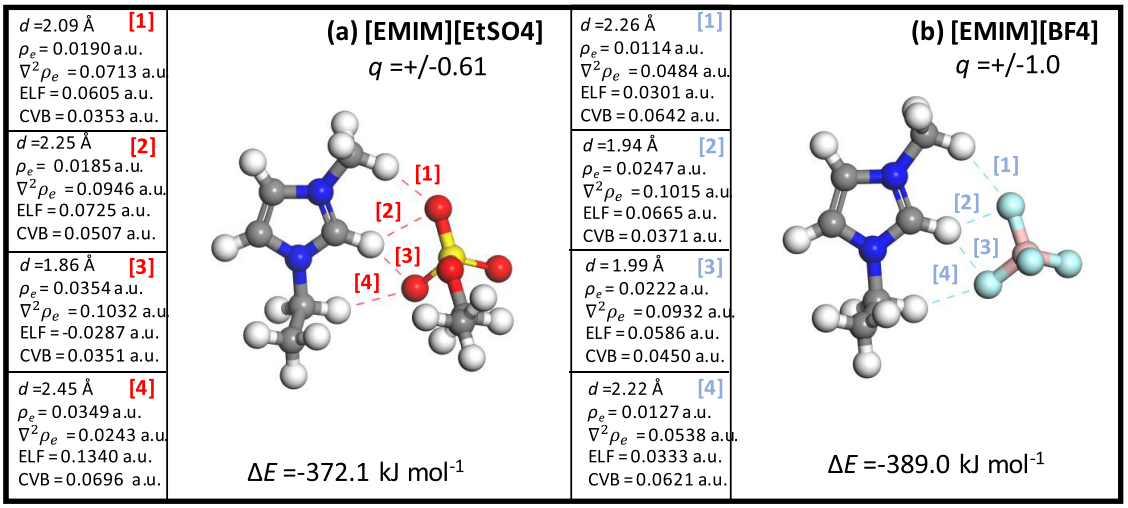

Figure 6. DFT optimized structures of [EMIM]−[EtSO4] and [EMIM]−[BF4] 1:1 clusters showing the lowest energy configurations including binding energy, ΔE, QTAIM properties (electronic density, ρ_e, and Laplacian of electron density, $\nabla^2\rho_e$), electron localization function (ELF), core valence bifurcation index (CVB), all these properties reported at the bond critical point (BCP) and region corresponding to the reported hydrogen bonds (dashed lines). Total cation and anion (ChelpG) charges are also reported, q.

one type of anion on the structuring of the other, thus leading to new intermolecular interactions upon anion replacements.

The small changes in intermolecular forces upon mixing are confirmed by the mixture composition evolution of the calculated VFT parameters. The VFT A and B parameters (Figure 4a,b) follow a linear trend with mixture mole fraction, and the T_0 parameter (Figure 4c), which is related to the glass transition temperature, evolves through a nonlinear relationship, remaining constant from neat [EMIM][EtSO4] to almost equimolar mixtures. Nevertheless, it should be remarked that the difference between the T_0 of both pure ILs is just 7 K. Therefore, these VFT parameters indicate that the changes in intermolecular forces arise just from the dilution of each type of IL in the second one upon concentration changes, without large changes in the nature of each cation−anion interaction.

Further details on the intermolecular forces in the considered IL mixtures may be inferred from the information obtained from the PFP[21] modeling of V^E (Figure 5), which allows to

https://doi.org/10.1021/acs.iecr.4c02839
Ind. Eng. Chem. Res. 2025, 64, 1774−1791

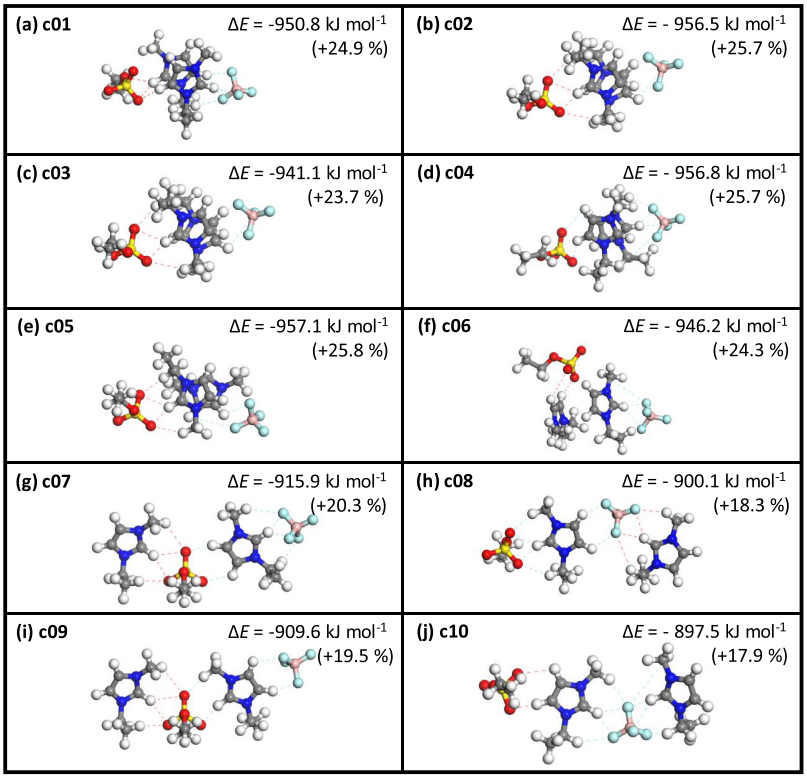

Figure 7. DFT optimized structures and binding energy, ΔE, for (1) [EMIM] − (1) [EtSO4] + (1) [EMIM] − (1) [BF4] clusters, considering different molecular orientations. Parenthesized percentage values indicate the difference between the binding energy per cluster and the sum of each dimer from the results in Figure 6.

connection of the macro and microscopic information. Results in Figure 5A show that the PFP model is able to describe V^E with a single fitting parameter, χ_{12} (Figure 5b). The small values for χ_{12}, linearly decreasing with temperature, show again the minor changes in intermolecular forces upon mixing.[51,52] The PFP analysis of V^E allows us to infer three contributions: interactional, free volume, and P^* contributions. It is remarkable that free volume contribution is almost negligible, with the interaction being negative and P^* being positive and slightly larger leading to the minor positive V^E. Therefore, the newly developed intermolecular forces developed upon mixing (negative χ_{12}, Figure 5b) are produced in minor extension (small negative interactional contribution, Figure 5c) and are mostly balanced by the positive P^* contributions paired with almost negligible free volume contribution (Figure 5d). The P^* contribution stands on the differences in internal pressures and reduced volumes of the components upon mixing,[53] this positive effect reported in Figure 5e confirms that changes upon mixing rise in the reorganization of molecules with the minor extension of new interactions (Figure 5b,c).

3.2. On the Nature of Hydrogen Bonding. Experimental thermophysical properties reported in the previous section allowed us to characterize the macroscopic behavior from the thermodynamic viewpoint and also infer pivotal features of the fluids' nanoscopic properties. Further analysis of the nature of the mixed fluids was carried out through the consideration of intermolecular forces (hydrogen bonding) via DFT calculations, considering model molecular clusters for neat ILs and mixed ILs. In the first stage, dimers formed by [EMIM]: [EtSO4] and [EMIM]: [BF4] in 1:1 combinations were considered, with their main properties reported in Figure 6. Although the dimer model is a limited representation of ILs, it provides relevant information on the short-range cation−anion interactions mainly via neat Coulombic and hydrogen bonding. The ΔE values reported in Figure 6 indicate strong cation−anion interactions for both anions, with a very minor effect on the type of anion. The similar strength of interaction with [EMIM] both for [EtSO4] and [BF4] would be on the root of the minor changes in ideality, as reported in the previous section, i.e., the binary mixed IL in which the concentration of one type of anion decreases whereas the concentration for the other one increase does not lead to remarkable changes in the anion−cation interaction energy, thus, minor changes in energy-related properties of the fluid as a function of composition. The main anion-[EMIM] interaction is developed via hydrogen bonding through the C(1) site in the imidazolium ring (the −CH site between the two N atoms) but also the anions are able to interact with the hydrogen atoms in the neighbor alkyl sites, thus leading to very strong anion−cation interactions through the four interacting sites, Figure 6. Regarding the Coulombic interaction, results for [EMIM]−[EtSO4] show lower ionic charges than for [EMIM]−[BF4], i.e., stronger Coulombic interactions for the spherical [BF4] anion. This also leads to slightly shorter hydrogen bonds with the cation for [BF4], interactions [2] and [3] in Figure 6.

The QTAIM analysis of cation−anion interactions via ρ_e and $\nabla^2\rho_e$ for the type (3,−1) BCPs developed in the hydrogen bonding paths ([2] and [3] interactions in Figure 6) and for the interaction with the alkyl groups ([1] and [4] in Figure 6). It should be remarked that 0.002 au < ρ_e < 0.04 au and 0.02 au < $\nabla^2\rho_e$ < 0.139 au ranges correspond to interactions that can be classified as shared-based interactions or H-bond established between the attraction sites, with larger values indicating stronger interactions.[54] The ρ_e and $\nabla^2\rho_e$ for H-bond interactions

https://doi.org/10.1021/acs.iecr.4c02839
Ind. Eng. Chem. Res. 2025, 64, 1774−1791

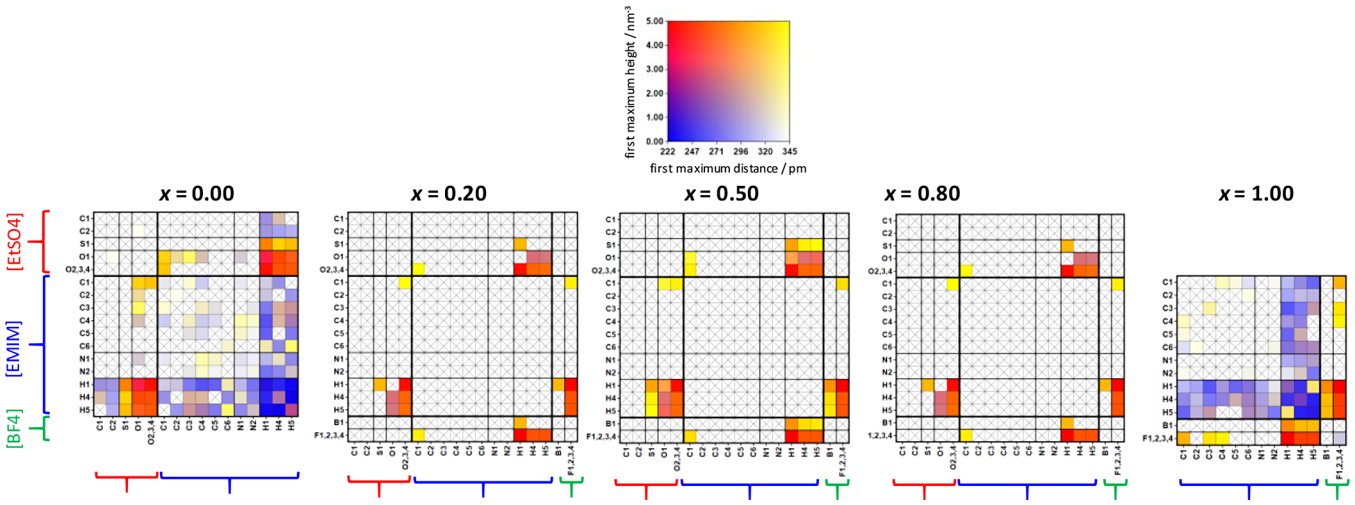

Figure 8. Connection matrix analysis of interactions in x [EMIM][BF4] + $(1 - x)$ [EMIM][EtSO4] mixtures, where et is for mole fraction, from MD simulations at 303 K and 1 bar. Atom labeling as in Figure 1.

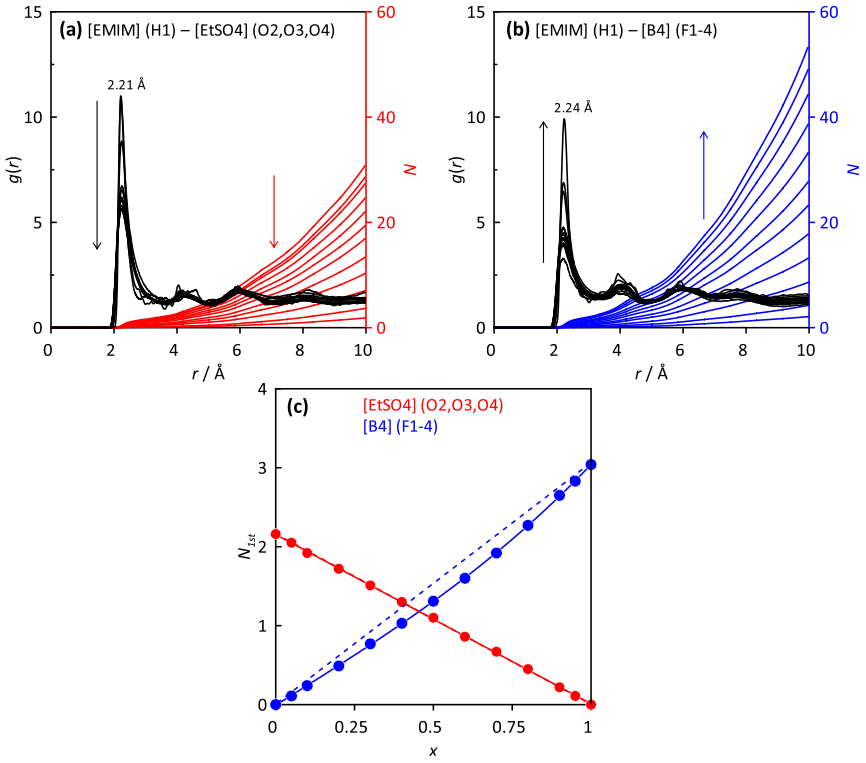

Figure 9. (a, b) Center-of-mass radial distribution function, $g(r)$, and the corresponding solvation number, N, in x [EMIM][BF4] + $(1 - x)$ [EMIM][EtSO4] mixtures, where m stands for mole fraction, from MD simulations at 303 K and 1 bar. Arrows indicate increasing mole fraction for the compositions reported in Table S8 (Supporting Information). (c) N values for the radial distribution function first peak ($r < 3.60$ Å). In panel c, dashed lines indicate linear behavior for comparison purposes. Atom labeling as in Figure 1.

([2] and [3] in Figure 3) indicate the formation of strong interactions for both anions and the presence of two simultaneous interactions on the C(1) [EMIM] site contributes to large anion−cation interactions. Likewise, anion−cation interactions through the alkyl sites in [EMIM] ([1] and [4]) although weaker than those through C(1) are also strong, thus contributing to the stabilization of cation−anion pairs. The strength of anion−cation intermolecular interactions is also quantified via CVB and ELF, which indicate moderately strong interactions.

Beyond the minimal anion−cation dimers considered as initial models of isolated clusters, the effect of mixing in the considered H-bonding was analyzed via DFT considering tetramers formed by the association of dimers reported in Figure 6 considering different mechanisms of interaction, i.e., spatial arrangements with particular orientations. These tetramers, resembling equimolar [EMIM][EtSO4] + [EMIM]-[BF4] clusters, were considered in ten different orientations, the optimized structures of which are reported in Figure 7. For all the cases, large ΔE values are inferred in all the cases, with the values for the tetramer being larger than the addition of those for

https://doi.org/10.1021/acs.iecr.4c02839
Ind. Eng. Chem. Res. 2025, 64, 1774−1791

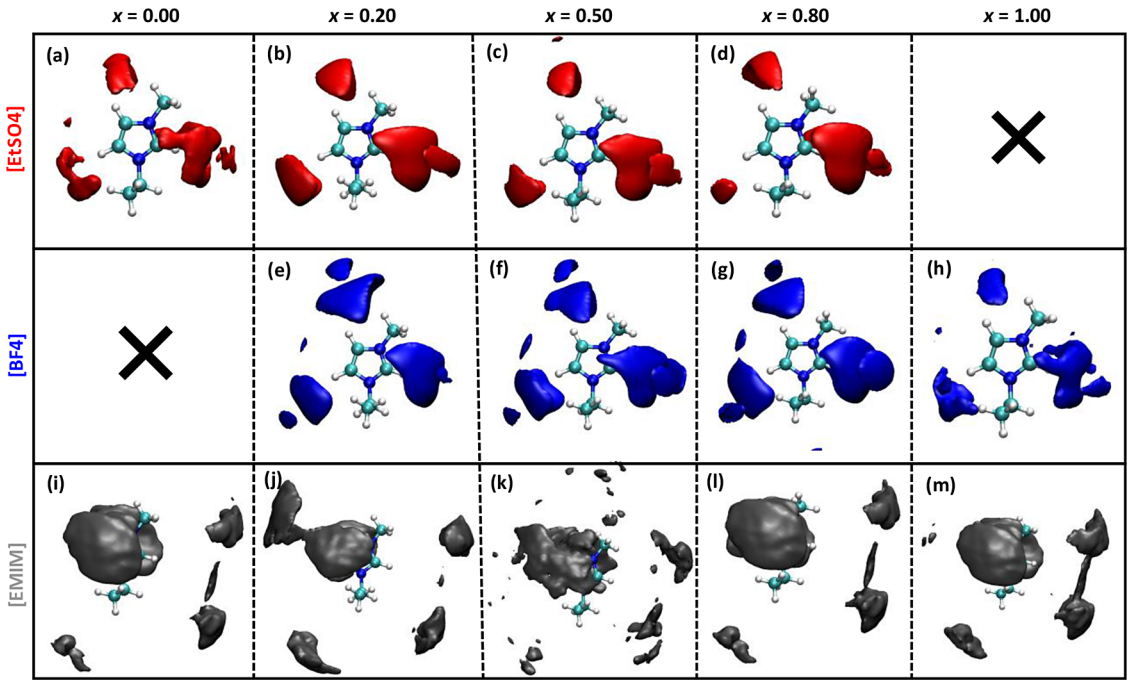

Figure 10. Spatial Distribution Functions around central [EMIM] cation for the reported molecules: [EtSO4] (O2−4 atoms), [BF4] (F1−4 atoms) and [EMIM] (C1 atoms) in x [EMIM][BF4] + (1 − x) [EMIM][EtSO4] mixtures, where stands for mole fraction, from MD simulations at 303 K and 1 bar.

the dimers, i.e. new intermolecular forces are formed upon tetramer formation leading to increases in ΔE values in the range of 18−26%. Therefore, the formation of larger clusters of the replacement of a type of anion for another one in the neighbor cluster does not lead either to a disrupting effect or to a decrease in the cluster (H-bonding) stability but, on the contrary, to additional stabilization. Likewise, the ten different orientations reported in Figure 7 show ΔE with minor differences between them (∼58 kJ mol^{-1}), thus confirming a large versatility of the arrangements between neighbor ionic pairs leading to stable configurations, which would be on the roots of the thermodynamics macroscopic behavior.

3.3. Nanoscopic Characterization of Mixed Liquid Phases. The model clusters reported in the previous section provide information on the nature of H-bonding in the considered systems, but liquid structuring is also characterized by additional effects like long-range interactions, molecular packing, and dynamic evolution, which require considering larger model systems being studied using MD simulations. The suitability of the considered force field used for MD simulations is analyzed via the comparison of (relevant) experimental properties (density and dynamic viscosity; Figure S1, Supporting Information). The MD-predicted density and viscosity data are lower than the experimental ones, but the deviations for density (1.2% on average) and viscosity (19.1% on average) are reasonable considering the purely predictive nature of the MD approach. Likewise, the evolution of density and viscosity with mixture composition is in reasonable agreement with experimental behavior, and thus, the considered MD approach may be considered as a suitable representation of the considered mixed fluid properties and structuring.

The first analysis of the studied IL mixtures was carried out considering structuring. The possible donor−acceptor sites were analyzed via Radial Distribution Functions (RDFs), which were systematically arranged considering the so-called connection matrix (*cmat*), in which RDFs for relevant interacting pairs are calculated, the first RDF peak being calculated in terms of its distance and intensity and assigned a color code, thus inferring the most relevant intermolecular interactions, Figure 8. The reported *cmat* results discard [EMIM]−[EMIM] self-association and confirm cation−anion interaction. The cation−anion interaction is mainly developed (red spots in Figure 8) through the cation C(1) sites, whereas interactions through the [EMIM] C(2) sites (opposite sites in imidazolium ring) also being present are produced in lower extension (orange spots in Figure 8). This pattern of interaction is maintained in the whole composition range, and when both anions are present in the mixture they provide the same mechanism of interaction being a combination of those of neat ILs, thus proving that the model clusters considered for DFT studies (Figure 7) are representative of the mechanism of interaction and that the liquid mixture structure is mainly characterized by a continuous replacement of one type of anion by the other one, without large disruptions of the liquid phase structuring and thus leading to minor deviations of thermodynamic ideality.

Particular details of the cation−anion interactions via the main interaction site C(1) in the imidazolium ring are reported in Figure 9 considering RDFs. The RDFs are almost equivalent for both types of anions (Figure 9a,b) following a first very intense RDF peak corresponding to H-bonding followed by weak peaks at larger distances, i.e., cluster models in Figures 6 and 7 represent the mechanism of H-bonding. The maximum of the first RDF peak appears at the same distance for both anions and their intensity changes upon changing anion concentration without changes in the position, i.e., indicating again an anionic replacement mechanism. The integration of the first peak of RDFs leads to the number of anions around the [EMIM], N_{first}, which are plotted as a function of mixture composition in Figure 9c. In the case of [EtSO4], N_{first} evolves in a linear way with composition, and for the case of [BF4] N_{first} evolves in a

https://doi.org/10.1021/acs.iecr.4c02839
Ind. Eng. Chem. Res. 2025, 64, 1774−1791

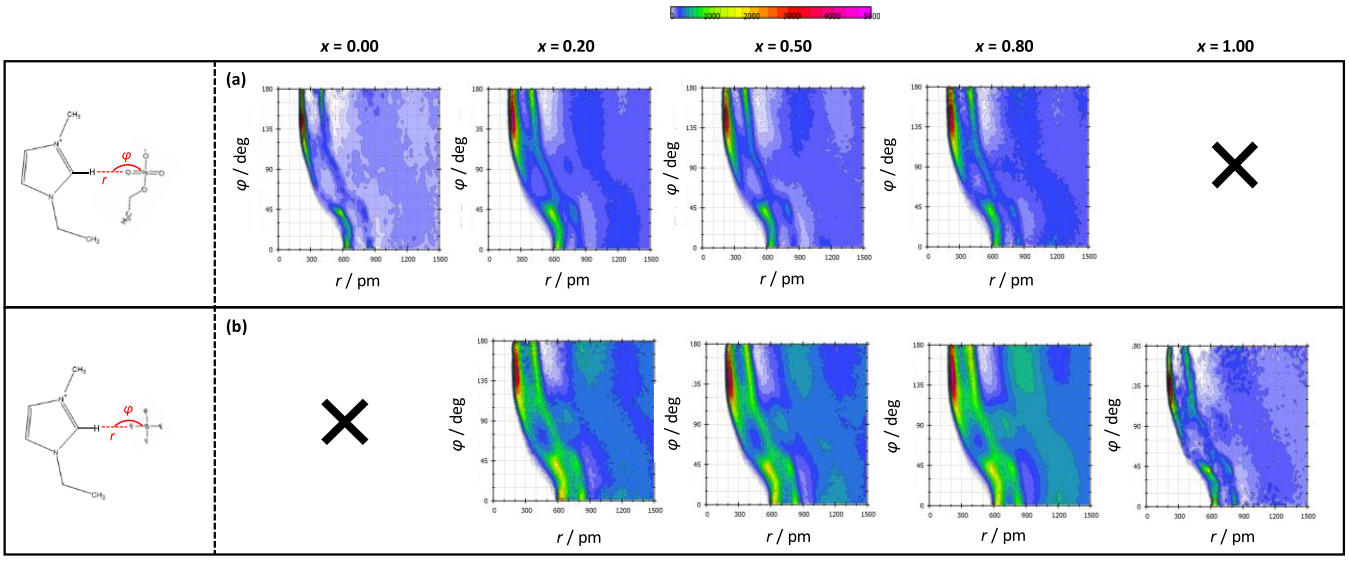

Figure 11. Combined Distribution Functions for the distance and angles between relevant sites in x [EMIM][BF4] + $(1 - x)$ [EMIM][EtSO4] mixtures, where the asterisk stands for mole fraction, from MD simulations at 303 K and 1 bar.

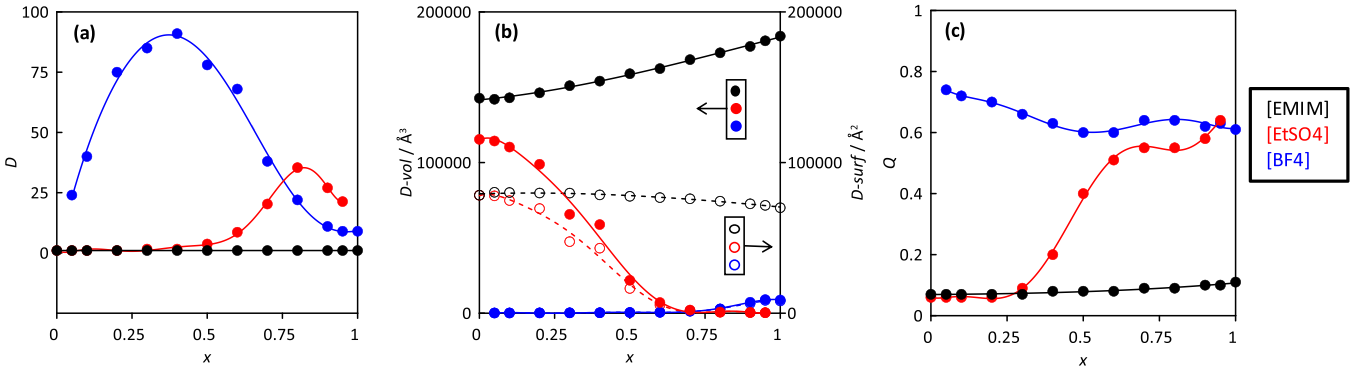

Figure 12. Domain analysis in x [EMIM][BF4] + $(1 - x)$ [EMIM][EtSO4] mixtures, where "Mole fraction" stands for, from MD simulations at 303 K and 1 bar. Number of domains, *D*, average domain area, *D-surf*, volume, *D-vol*, and isoperimetric index, *Q*, are reported. Atom labeling as in Figure 1.

nonlinear way with a lower number of [BF4] anions than expected from composition; this deviation is not too large and confirms the replacement of one type of anion by the other one around the cation upon mixing in a ratio corresponding to the mixture composition.

The distribution of anions around the [EMIM] cation is analyzed via spatial distribution functions (SDFs), Figure 10. SDFs indicate that both anions are mainly placed around the C(1) site of [EMIM] and non-negligible distributions are also produced around the C(2) sites, corresponding to the interaction between neighbor anion−cation clusters. It is remarkable that both anions show an analogous distribution around the cation, which is maintained throughout the whole composition range. Likewise, the interaction between neighbor [EMIM] cations is characterized by a distribution on top of the imidazolium ring, in this way allowing anion−cation effective interactions as well as ring−ring interactions between neighbor [EMIM] cations leading to additional stabilization factors in terms of van der Waals interactions as well as to more effective molecular packing, and thus densification.

The geometrical nature of the developed H-bonds is analyzed via the combined distribution functions (CDFs) considering interatomic separation and angle between relevant sites (around C(1) in [EMIM]), Figure 11. It is remarkable that the hydrogen bonding is confirmed considering a geometrical criterion (red spot in Figure 11) and exactly the same pattern for CDFs is inferred for the considering anions and the whole concentration range, i.e. almost negligible effect of mixture composition is inferred in the hydrogen bonding and interionic orientation.

Beyond the anion−cation intermolecular forces, analysis of the liquid phase properties is carried out considering long-range molecular distribution and clustering on the considered mixtures through the domain analysis reported in Figure 12. Although negligible changes upon mixing are inferred from the analysis of intermolecular forces previously discussed, results for domains reported in Figure 12 show subtle changes. In the case of [EMIM] domains, the domain count shows a single domain along the whole fluid, indicating a large interconnection between cations in agreement with the spatial distribution reported in Figure 10i−m, which showed cation to cation (top on top) orientation. The size of this [EMIM] domain increases with [BF4] content, which corresponds to an increase in density on going from [EtSO4] to [BF4] (Table S1, Supporting Information). Regarding anion domains, results for [EtSO4] show a lower number of domains than for [BF4] in the [EtSO4]−rich region (low x) and vice versa for the [BF4] rich region. Nevertheless, the size of [EtSO4] domains is mostly lower than those for [BF4], mainly because of the large anion

https://doi.org/10.1021/acs.iecr.4c02839
Ind. Eng. Chem. Res. 2025, 64, 1774−1791

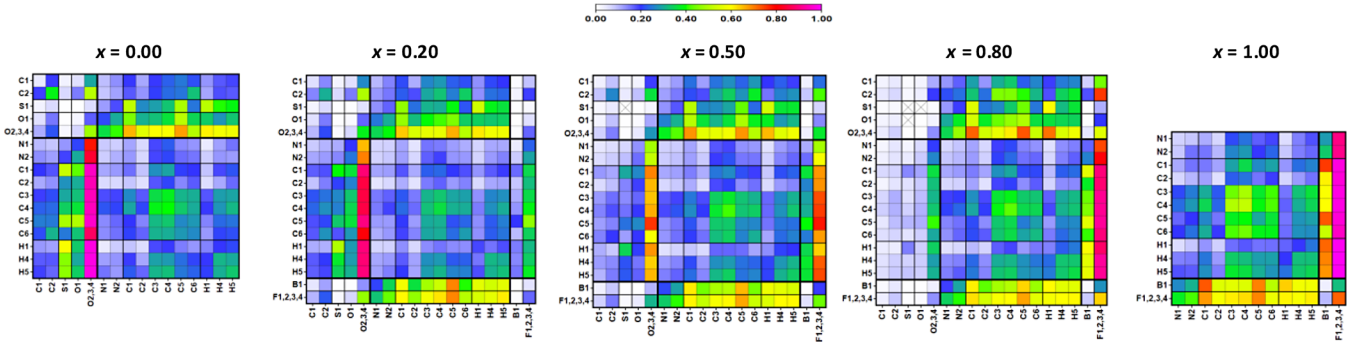

Figure 13. Neighbor probability matrix from Voronoi analysis in x [EMIM][BF4] + $(1 - x)$ [EMIM][EtSO4] mixtures, where the letter "Et" stands for mole fraction, from MD simulations at 303 K and 1 bar. Atom labeling as in Figure 1.

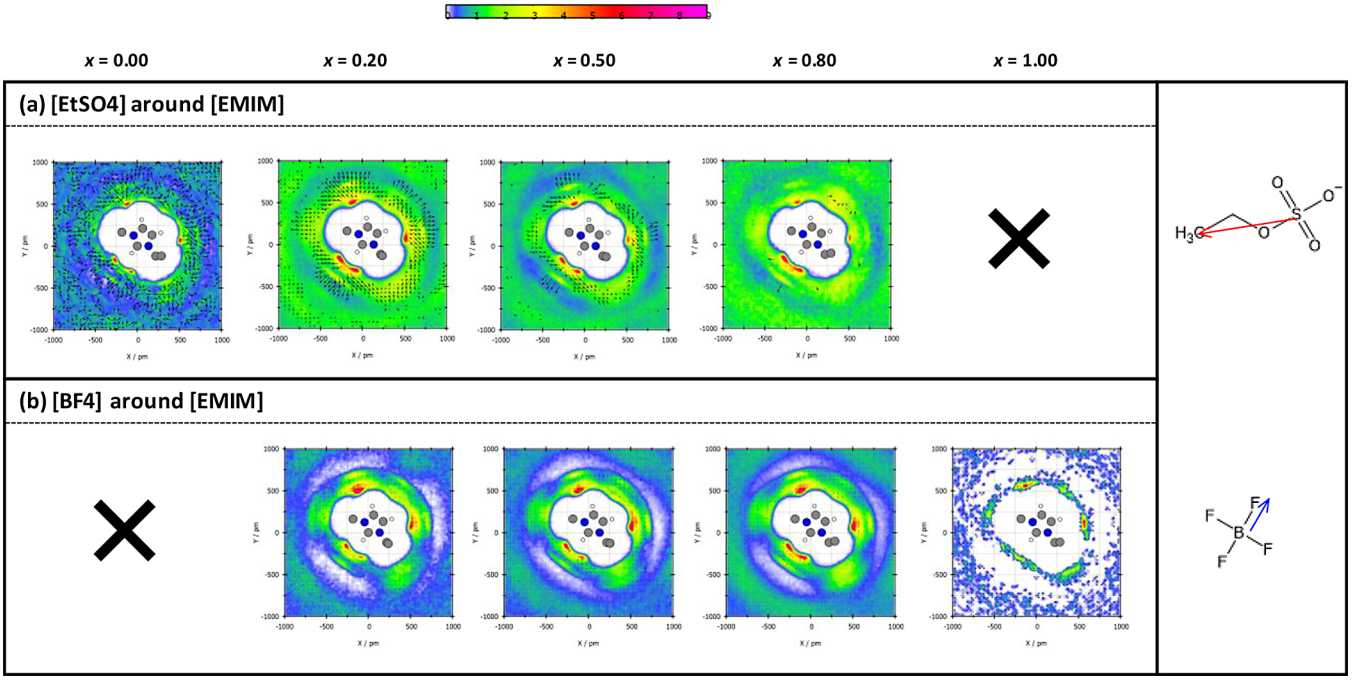

Figure 14. Average particle density of the reported molecules around a central [EMIM] molecule in x [EMIM][BF4] + $(1 - x)$ [EMIM][EtSO4] mixtures, where the "mean atomic mass" stands for mole fraction, from MD simulations at 303 K and 1 bar. Average orientation of the reported vectors is also indicated.

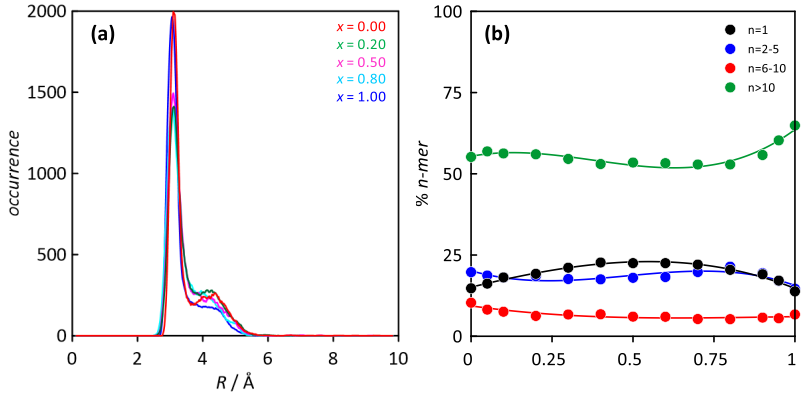

Figure 15. Cluster analysis for cation - anion aggregation in x [EMIM][BF4] + $(1 - x)$ [EMIM][EtSO4] mixtures, where stands for mole fraction, from MD simulations at 303 K and 1 bar. (a) Results show occurrence of possible clusters as a function of distance, R. (b) Percentage distribution of the cluster composed of n molecules (n-mers).

size. The evolution of anion domains follows a nonlinear trend increasing up to a value, i.e., declustering, and then decreasing reclustering. These effects point to a mechanism of anionic replacement which forces the connection of anion domains of

https://doi.org/10.1021/acs.iecr.4c02839
Ind. Eng. Chem. Res. 2025, 64, 1774−1791

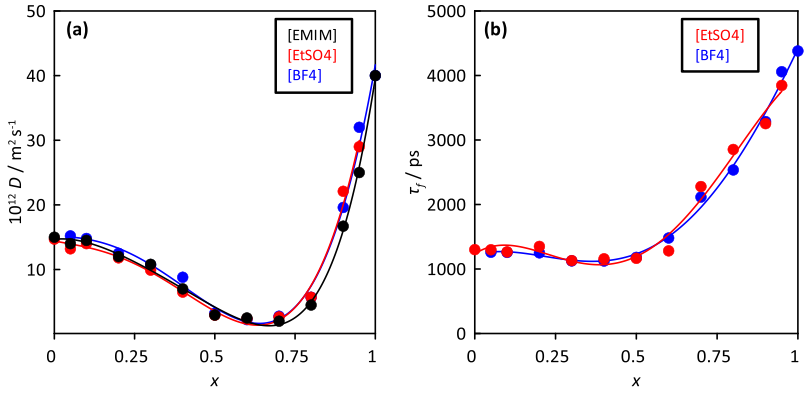

Figure 16. (a) Center-of-mass self-diffusion coefficient, D, and (b) living times of ion pairs, τ_f, for the considered ions in x [EMIM][BF4] + (1 − x) [EMIM][EtSO4] mixtures, where the word "mole fraction" stands for mole fraction, from MD simulations at 303 K and 1 bar.

the same type when the other anion prevails, i.e., anion microdomains leading to certain nanoscopic heterogeneity. Likewise, a relevant structural feature appears from the cationic interconnection, which determines the fluids' structure in which anions are distributed in the available sites around the C(1) imidazolium sites. The anionic domains show a certain degree of sphericity, especially changing the shape for those involving [BF4] anion, Figure 12c. Further analysis of the possible clustering is carried out through the neighbor probability matrix reported in Figure 13. These matrices show a similar interatomic distribution function in the whole considered composition range, and they may be considered as a fingerprint of the atom-to-atom distribution in the liquid phases, i.e. confirming analogous site-to-site distribution independently of the type of anion, thus pointing again to the anion per anion replacement mechanism for describing mixture properties.

The orientation of anions in the solvation shells around the [EMIM] cation is analyzed in Figure 14. Both types of anions show similar orientation around the cation C−H imidazolium sites (red spots). Likewise, anion vectors are highly oriented around the H-bonding imidazolium sites, especially for the [EtSO4] anion, in which the sulfate group is totally oriented toward the ring whereas the spherical shape of [BF4] provides a larger flexibility around the cation. This effect would be on the root of the lower density for [EtSO4] than for [BF4].

The anion−cation clustering is analyzed in Figure 15. Results in Figure 15a report cluster size distribution as a function of mixture composition, showing almost the same distribution in the whole composition range, i.e. changing the type of anion does not remarkably change the size of clusters, and only one type of anion is replaced by the other one. The two main peaks in Figure 15a correspond to clusters with 3.1 and 4.4 Å radii, being an anion−cation dimer (n = 1) or tetramer (n = 2). The first peak corresponding to n = 1 shows almost negligible changes upon mixing, whereas the second (weaker) one slightly decreases with increasing [BF4], but the most relevant features of cluster size are maintained in the whole composition range. Further analysis was carried out considering the percentage distribution of each type of cluster starting from n = 1 (1:1 anion−cation pair), as the simplest and smallest association, and increasing the number of ions in the cluster, Figure 15b. The first relevant conclusion stands on the large percentage of clusters with n > 10, which agreed with the domain distribution reported in Figure 14a, considering the interconnection between the cations. Therefore, liquid structuring is characterized by large clusters connected anion to cation via hydrogen bonding and through additional interactions among neighbor pairs (Figure 7). The cluster distribution shows subtle changes with mixture composition, but the most relevant features are analogous in the whole composition range, i.e., the mechanism of ionic aggregation and distribution remaining almost constant when one type of anion is gradually replaced by the other one.

The dynamic properties of the mixed ILs were first analyzed considering the self-diffusion coefficients, D, as calculated from the mean square displacement (MSD) and Einstein's equation, Figure 16a. The first remarkable result stands for the equal D values for the cation and anions at each fixed composition. This pairing of ionic movement comes from the development of anion−cation interactions, clustering, and through the replacement of a type of anion by the other one, leading to paired [EtSO4] and [BF4] diffusion. The composition evolution of D is largely nonlinear, in agreement with the experimental behavior of viscosity, Figure 2e,f. The D values for pure [EMIM][EtSO4] are lower than those for pure [EMIM][BF4], corresponding to larger viscosities for [EtSO4] containing fluids. These lower diffusion could be explained considering that [EtSO4] participates in larger domains than [BF4], Figure 12, and although anion−cation interactions have almost the same strength for both types of anions, Figures 6 and 7, the larger domains hinder ionic diffusion, thus leading to larger viscosity. The nonlinear evolution of D with mixture composition evolves through a minimum at [BF4] rich composition and then a sharp increase up to neat [EMIM][BF4]. The initial decrease of D for the [EtSO4] rich region with [BF4] increasing concentration may rise by the dispersion of [BF4] anions in the large [EtSO4] domains, Figure 12a. This increasing concentration of isolated [BF4] domains will decrease ionic mobility for all the considered ions. As the [BF4] rich region is reached, larger [BF4] prevailing domains are formed, which move faster, i.e. increasing global ionic motion. Therefore, ionic mobility and domains and clustering evolution with composition evolution are largely correlated.

Additionally, the dynamic properties of H-bonding are analyzed considering reactive flux analysis,[55] which leads to the hydrogen bonding lifetime (so-called forward process, τ_f), Figure 16b. This analysis shows very stable H-bonds with longer lifetimes for [BF4]−rich mixtures. Likewise, for each fixed composition, the lifetimes of each type of hydrogen bond are the same, which again points to the replacement mechanism as the feature controlling the nanoscopic structuring. Almost negligible changes in lifetimes are produced up to equimolar compositions, i.e., [EtSO4]−rich mixtures, and then a further increase in

https://doi.org/10.1021/acs.iecr.4c02839
Ind. Eng. Chem. Res. 2025, 64, 1774−1791

lifetimes with [BF4] enrichment. This effect can be justified considering the domain distribution reported in Figure 12a; for the [EtSO4]-rich region, almost a continuous domain is produced connecting cations and anions (domain count close to unity), and this facilitates H-bonding breaking and reforming. Upon the increase of the [BF4] content, the number of anion domains increases, thus hindering H-bonding reforming. Nevertheless, these dynamic features agree with experimental behavior and show how structuring and dynamic properties are intimately connected, and thus not only is the mechanism of interionic interaction relevant but also the long-range ionic distribution pivotal for determining ionic mobility, although intermolecular forces remain almost constant upon mixing.

3.4. Interaction with Biomolecules and Cell Membranes. The possible biological effects (i.e., toxicity) of the considered ILs and IL mixtures are first analyzed considering their interaction with a model lipid bilayer formed by DPPC lipids to mimic the interaction of the considered ILs with cell walls. Literature studies on the interaction of ILs with lipid bilayers are scarce, Yoo et al.[56] probed via MD simulations imidazolium cationic insertion into model POPC bilayers leading to surface roughening as the precursor of bilayer disruption, and additional perturbation effects have been reporting being indicative of toxic effect of mainly imidazolium−based ILs.[57,58] Nevertheless, these studies considered neat ILs not mixed ILs, and, in most of the cases, low IL concentration. Results in Figure 17 show DPPC bilayer structuring in the presence of the considered IL mixtures. Both for pure ILs as well as for the considered mixtures, large bilayer roughness is induced, which confirms the roughness previously reported[54] being exacerbated by the larger concentration considered in this work. Although the bilayer integrity is maintained upon interaction with ILs, the roughening is induced by the adsorption of ions on the outer polar region of the lipids. Likewise, there is a clearly different preferential adsorption arrangement with [BF4] anions placed in outer regions close to the head choline groups, whereas [EtSO4] and mainly [EMIM] cations penetrate inside the bilayer remaining closer to the phosphate and glycerol groups, respectively. All of the considered ions remain in the top polar region of the bilayer surface without staying in the apolar central region. Surface roughening is maintained and shows similar characteristics for all the considered composition effects, with the anion exchange scheme pointing to a larger amount of ions on the outer layer for [BF4]-rich mixtures, whereas for [EtSO4]-rich mixtures, a larger ionic concentration is inferred in inner regions of the polar heads. In all the cases, the presence of [EMIM] inside the polar region leads to a largely disruptive effect on the surface roughness. This increase in the surface curvature is produced by the large affinity of the considered ions for the polar head groups of the lipids, which through increasing roughness leads to an improvement of ion−lipid interactions both in terms of extension and strength. The perturbation of bilayer properties is quantified considering bilayer width and Area Per Lipid (APL) taking as reference the calculated bilayer properties in the absence of ILs; Figure 18a. In most of the cases, the presence of the ILs leads to a bilayer expansion (with the exception of neat [EMIM][BF4] in the three space directions (increase of width and APL), which is produced for the accommodation of strongly interacting ions. There is not a clear effect on the content of anions, although the presence of [BF4] seems to decrease the perturbative effects because the spherical symmetry and size of these anions allow better surface accommodation with lower

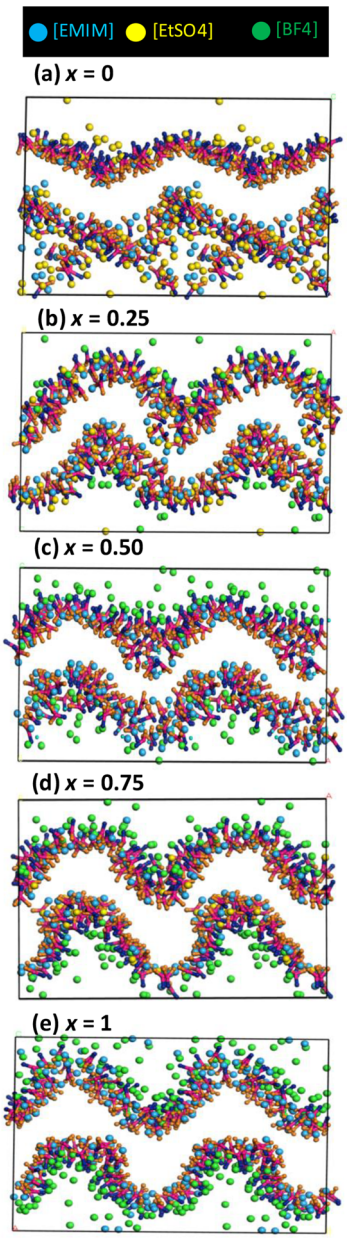

Figure 17. Results of Coarse Grained MD simulations of x [EMIM][BF4] + $(1 - x)$ [EMIM][EtSO4] mixtures in aqueous solution (Table S9, Supporting Information) in contact with the DPPC lipid bilayer at 313 K. Snapshots at the end of the simulations are reported. Lipid alkyl chains as well as water molecules are omitted for the sake of visibility.

bilayer disruption. The strong ion−(polar head) lipid interactions decrease lipid mobility, as probed by the decrease in lateral diffusion reported in Figure 18c, i.e., ions adsorption on the surface modifies both the structural and dynamic properties (fluidity) of the bilayer, which indicate a large disrupting effect. Nevertheless, considering that ion interaction is produced in the polar head regions of the bilayer, perturbations on the apolar regions are almost negligible as probed by the minor changes in lipid extension and internal angle reported in Figure 19. The mechanism of ion-polar head interactions is quantified through the corresponding RDFs reported in Figure 20, where it is clearly proved that the [EMIM] cation interacts mainly with internal phosphate and glycerol, [BF4] with external choline, and

https://doi.org/10.1021/acs.iecr.4c02839
Ind. Eng. Chem. Res. 2025, 64, 1774−1791

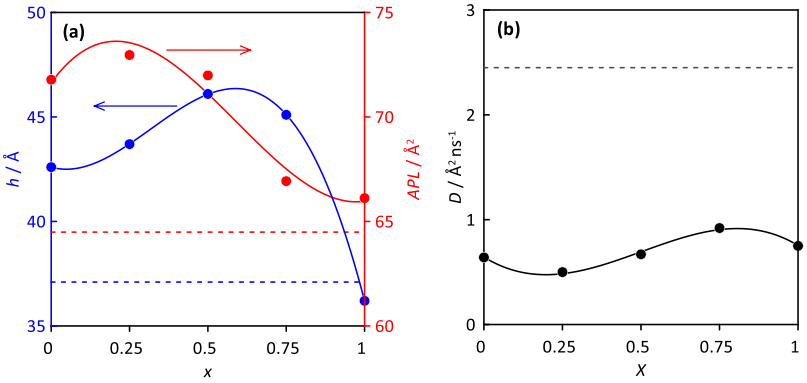

Figure 18. Results of Coarse Grained MD simulations of x [EMIM][BF4] + $(1 - x)$ [EMIM][EtSO4] mixtures in aqueous solution (Table S9, Supporting Information) in contact with DPPC lipid bilayer at 313 K. (a) Lipid bilayer width, h, defined as the distance between NC groups (choline group) in top and bottom layers and APL standing as Area per Lipid; (b) lateral self-diffusion coefficients, D, for DPPC lipids. Dashed lines in each panel show the values for the DPPC bilayer in contact with the water layer in the absence of ILs.

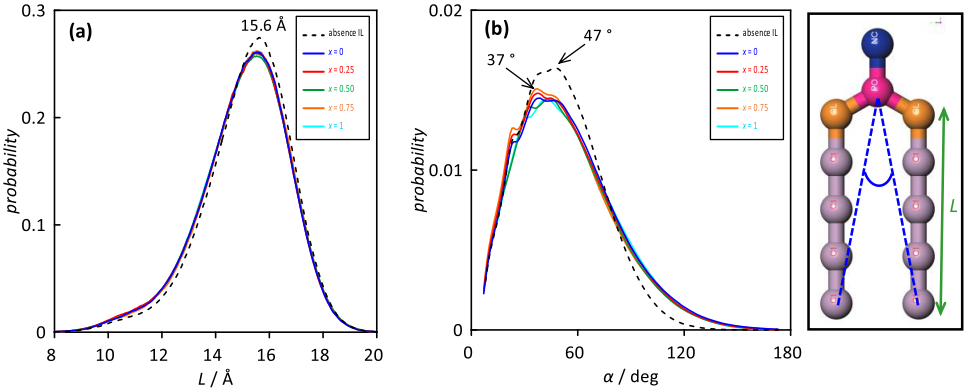

Figure 19. Results of Coarse Grained MD simulations of x [EMIM][BF4] + $(1 - x)$ [EMIM][EtSO4] mixtures in aqueous solution (Table S9, Supporting Information) in contact with the DPPC lipid bilayer at 313 K. Results indicate probability distributions of geometrical properties of DPPC lipid in the bilayers.

[EtSO4] remaining in a central region being able to interact with all the groups. These results indicate that for a mixed IL containing [BF4] and [EtSO4] anions, both types of anions do not compete for the adsorption regions on the lipid polar surfaces, whereas they adsorbed in different regions, being also different from those of [EMIM] cation, and thus, the anionic effect on lipid bilayer disruption would be additive and synergistic, leading to larger toxic effects.

Additional possible toxic effects of the considered ILs were analyzed by doing docking studies on four model proteins for ion clusters reported in Figure 7, as models of mixed ILs interacting with different biological targets. The results in Figure 21 provide the biomolecule−cluster interaction energies. Docking interaction energies are in the −6 to −21 kcal mol^{-1}, which indicates favorable ionic cluster−biomolecule interaction, i.e. non-negligible biological effects that may be related, at least qualitatively with possible toxic effects. For a fixed cluster configuration, there is not a remarkable effect on the type of biomolecule, indicating that ion pairs are able to reach the most stable configuration independently of the biomolecule. Nevertheless, results indicate that there is a large effect on the type of considered clusters leading to very different interactions with the biomolecule both in terms of mechanism(s) and strength. Therefore, these results combined with those for the interaction with lipid bilayers point to aremarkable interaction of the considered mixed ILs with biosystems, pointing to non-negligible toxic effects, exacerbated through synergistic effects by the presence of different types of anions, which should be taken into account for the large-scale application of complex multicomponent IL mixtures.

4. CONCLUSIONS

In this research, our primary focus was the comprehensive examination of [EMIM][BF4] and [EMIM][EtSO4] ionic liquids and their binary mixtures from macroscopic to nanoscopic scales as well as their potential biological implications. Beginning with macroscopic investigations, density and viscosity measurements unveiled a remarkable trend attributed to the presence of hydrogen-bonded cluster structures. Analysis of excess properties provided valuable insights into the mixing behavior of these ILs, revealing minor deviations from ideality primarily driven by the rearrangement of molecular clusters within the available free space. Moreover, the study of excess partial molar volumes demonstrated symmetric behavior, affirming the minimal disruption of the IL structuring upon mixing. Our research also delved into the behavior of intermolecular forces, demonstrating that changes in these forces were predominantly a result of dilution effects, with little alteration in cation−anion interactions. Collectively, these findings significantly contribute to our understanding of IL behavior, offering valuable insights into its potential applications in the fields of chemistry and materials science.

Moving to the nanoscopic realm, molecular dynamics (MD) simulations enabled the exploration of mixed liquid phases. The

https://doi.org/10.1021/acs.iecr.4c02839
Ind. Eng. Chem. Res. 2025, 64, 1774−1791

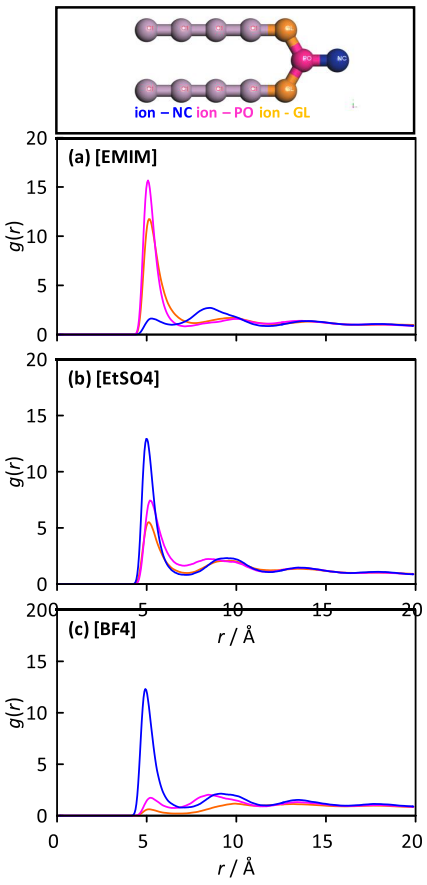

Figure 20. Results of Coarse Grained MD simulations of x [EMIM][BF4] + $(1 - x)$ [EMIM][EtSO4] (x = 0.5) mixture in aqueous solution (Table S9, Supporting Information) in contact with the DPPC lipid bilayer at 313 K. Results indicate radial distribution functions between the indicated ions and polar head groups in DPPC lipid in the bilayer.

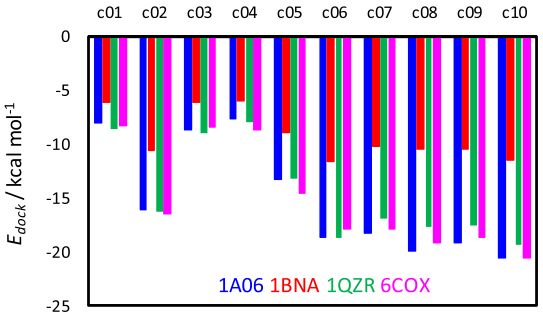

Figure 21. Results for the docking of IL clusters (Figure 7) into the reported biomolecules indicating IL−biomolecule affinity quantified as docking (interaction) energy, E_{dock}. E_{dock} values for the strongest interaction pose are reported in each case.

analysis uncovered robust cation−anion interactions at the C(1) and C(2) sites of [EMIM], with anion−cation replacement being the predominant structural mechanism. Spatial Distribution Functions illustrated consistent anion−cation interactions, substantiating structural stabilization and densification within these mixed liquid phases. Combined Distribution Functions further verified uniform hydrogen bonding geometry across anions and compositions, while domain analysis unveiled subtle nanoscale heterogeneity in anion domains. The study of cation−anion clustering revealed the enduring presence of large, hydrogen-bonded clusters, which remained consistent through various compositional variations. Additionally, dynamic properties, including self-diffusion coefficients and hydrogen bonding lifetimes, exhibited correlations with the observed viscosity behavior, demonstrating the interconnected nature of intermolecular forces, structural dynamics, and ionic mobility within these mixed liquid phases. These nanoscopic insights deepen our understanding of these systems, providing valuable knowledge for potential applications.

Expanding our scope to examine the potential biological effects, interactions with a model lipid bilayer, and docking studies on model proteins were conducted. Simulations uncovered the disruptive influence of both pure ILs and mixed ILs on the lipid bilayer, which induces significant roughening. Preferential adsorption of [BF4] anions near the choline groups and deeper penetration of [EtSO4] and [EMIM] cations into the bilayer were observed, underscoring the distinct behaviors of different ion types. Docking studies with model proteins indicated favorable interactions between ionic clusters and biomolecules, hinting at the potential biological effects. Importantly, the configuration of ion clusters played a crucial role in determining the nature and strength of these interactions, pointing to non-negligible toxic effects, possibly exacerbated by synergistic effects arising from the presence of various anion types.

This research not only advances our understanding of the fundamental behavior of ILs but also underscores the importance of considering the toxicological implications of complex multicomponent IL mixtures, particularly when they are employed on a large scale in diverse applications. The interactions observed with lipid bilayers and biomolecules emphasize the necessity for a comprehensive assessment of the biological effects of ILs in real-world scenarios, bridging the gap between fundamental research and practical applications.

From the viewpoint of industrial and technological relevance, this comprehensive study of [EMIM][BF4] and [EMIM][EtSO4] ionic liquids and their mixtures has significant implications. The insights gained into their macroscopic and nanoscopic properties can guide the development of tailored ILs for specific applications in chemistry and materials science. For instance, an understanding of viscosity trends and mixing behavior can inform the design of IL-based lubricants, electrolytes, and heat transfer fluids. The nanoscopic analysis of ion interactions and clustering behavior is crucial for optimizing ILs for use in catalysis, gas capture, and electrochemical devices. Furthermore, the revealed biological interactions are vital for assessing the environmental impact and safety of ILs in large-scale industrial processes. This knowledge can drive the development of safer, more efficient IL formulations for applications in pharmaceuticals, biomass processing, and green chemistry. Overall, this research provides a solid foundation for advancing IL technology across various sectors, balancing performance with safety considerations.

■ ASSOCIATED CONTENT

Supporting Information

The Supporting Information is available free of charge at https://pubs.acs.org/doi/10.1021/acs.iecr.4c02839.

Additional experimental and computational details, including thermophysical properties and molecular dynamics results (PDF)

https://doi.org/10.1021/acs.iecr.4c02839
Ind. Eng. Chem. Res. 2025, 64, 1774−1791

AUTHOR INFORMATION

Corresponding Authors

Santiago Aparicio − *Department of Chemistry, University of Burgos, 09001 Burgos, Spain;* orcid.org/0000-0001-9996-2426; Email: sapar@ubu.es

Jose L. Trenzado − *Department of Physics, University of Las Palmas de Gran Canaria, 35017 Las Palmas G.C., Spain;* Email: jose.trenzado@ulpgc.es

Author

Ylenia F. Rodríguez − *Department of Physics, University of Las Palmas de Gran Canaria, 35017 Las Palmas G.C., Spain*

Complete contact information is available at: https://pubs.acs.org/10.1021/acs.iecr.4c02839

Notes

The authors declare no competing financial interest.

ACKNOWLEDGMENTS

We acknowledge SCAYLE (Supercomputación Castilla y León, Spain) for providing supercomputing facilities. The statements made herein are solely the responsibility of the authors.

REFERENCES

(1) Walden, P. *Eber die Molekulargrösse und ElektrischeLeitfähigkeit Einiger Geschmolzenen Salze*; Benrath und Wainoff: 1914.

(2) Hurley, F. H.; Wier, T. P. The electrodeposition of aluminum from nonaqueous solutions at room temperature. *J. Electrochem. Soc.* **1951**, *98*, 207−212.

(3) Lei, Z.; Chen, B.; Koo, Y. M.; Macfarlane, D. R. Introduction: Ionic Liquids. *Chem. Rev.* **2017**, *117*, 6633−6635.

(4) Dong, K.; Liu, X.; Dong, H.; Zhang, X.; Zhang, S. Multiscale studies on ionic liquids. *Chem. Rev.* **2017**, *117*, 6636−6695.

(5) Philippi, F.; Rauber, D.; Eliasen, K. L.; Bouscharain, N.; Niss, K.; Kay, C. W.; Welton, T. Pressing matter: why are ionic liquids so viscous? *Chem. Sci.* **2022**, *13*, 2735−2743.

(6) Chen, Y.; Mu, T. Revisiting greenness of ionic liquids and deep eutectic solvents. *Green Chem. Eng.* **2021**, *2*, 174−186.

(7) Binnemans, K.; Jones, P. T. Ionic Liquids and Deep-Eutectic Solvents in Extractive Metallurgy: Mismatch Between Academic Research and Industrial Applicability. *J. Sustain. Metallurgy* **2023**, *9*, 423−428.

(8) Yadav, A.; Guha, A.; Pandey, A.; Pal, M.; Triveti, S.; Pandey, S. Densities and dynamic viscosities of ionic liquids having 1-butyl-3-methylimidazolium cation with different anions and bis-(trifluoromethylsulfonyl)imide anion with different cations in the temperature range (283.15 to 363.15) K. *J. Chem. Thermodyn.* **2018**, *116*, 67−75.

(9) Zhang, Q.; Zhang, S.; Deng, Y. Recent advances in ionic liquid catalysis. *Green Chem.* **2011**, *13*, 2619−2637.

(10) Macfarlane, D. R.; et al. Energy applications of ionic liquids. *Energy Environ. Sci.* **2014**, *7*, 232−250.

(11) Wang, M.; Zhang, L.; Gao, L.; Pi, K.; Zhang, J.; Zheng, C. Improvement of the CO2 absorption performance using ionic liquid [NH2emim][BF4] and [emim][BF4]/[bmim][BF4] mixtures. *Energy Fuels* **2013**, *27*, 461−466.

(12) Ventura, S. P. M.; Silva, F. A.; Quental, M. V.; Mondal, D.; Freire, M. G.; Coutinho, J. A. P. Ionic-liquid-mediated extraction and separation processes for bioactive compounds: past, present, and future trends. *Chem. Rev.* **2017**, *117*, 6984−7052.

(13) Zhou, Y. Ionic Liquids as Lubricant Additives-a Review. *ACS Appl. Mater. Interfaces* **2017**, *9*, 3209−3222.

(14) Zhou, F.; Liang, Y.; Liu, W. Ionic liquid lubricants: Designed chemistry for engineering applications. *Chem. Soc. Rev.* **2009**, *38*, 2590−2599.

(15) Xiao, H. Ionic Liquid Lubricants: Basics and Applications. *Tribol. Trans.* **2017**, *60*, 20−30.

(16) Zhou, W.; Zhang, M.; Kong, X.; Huang, W.; Zhang, Q. Recent advance in ionic-liquid-based electrolytes for rechargeable metal-ion batteries. *Adv. Sci.* **2021**, *8*, No. 2004490.

(17) de Castro, C. N. et al. Synthesis, properties and physical applications of ionanofluids. In *Ionic Liquids - New Aspects for the Future*; InTech, 2013.

(18) Pedro, S. N.; Freire, C. S. R.; Silvestre, A. J. D.; Freire, M. G. The role of ionic liquids in the pharmaceutical field: An overview of relevant applications. *Int. J. Mol. Sci.* **2020**, *21*, 8298.

(19) Chatel, G.; Pereira, J. F. B.; Debbeti, V.; Wang, H.; Rogers, R. D. Mixing ionic liquids-simple mixtures or "double salts"? *Green Chem.* **2014**, *16*, 2051−2083.

(20) Trenzado, J. L.; Rodríguez, Y.; Gutiérrez, A.; Cincotti, A.; Aparicio, S. Experimental and molecular modeling study on the binary mixtures of [EMIM][BF4] and [EMIM][TFSI] ionic liquids. *J. Mol. Liq.* **2021**, *334*, No. 116049.

(21) Shekaari, H.; Zafarani-Moattar, M. T.; Mokhtarpour, M.; Faraji, S. Volumetric and compressibility properties for aqueous solutions of choline chloride based deep eutectic solvents and Prigogine−Flory−Patterson theory to correlate of excess molar volumes at T = (293.15 to 308.15) K. *J. Mol. Liq.* **2019**, *289*, No. 111077.

(22) BIOVIA Dassault Systèmes. *Dmol3*; Dassault Systèmes: San Diego, 2022.

(23) Grimme, S.; Antony, J.; Krieg, H. A consistent and accurate ab initio parametrization of density functional dispersion correction (DFT-D) for the 94 elements H-Pu. *J. Chem. Phys.* **2010**, *132*, 154104.

(24) Simon, S.; Duran, M.; Dannenberg, J. How does basis set superposition error change the potential surfaces for hydrogen-bonded dimers? *J. Chem. Phys.* **1996**, *105*, 11024.

(25) Bogojeski, M.; Vogt-Maranto, L.; Tuckerman, M. E.; Müller, K. R.; Burke, K. Quantum chemical accuracy from density functional approximations via machine learning. *Nat. Commun.* **2020**, *11*, 5223.

(26) Bader, R. F. W. Atoms in molecules. *Acc. Chem. Res.* **1985**, *18*, 9−15.

(27) Lu, T.; Chen, F. Multiwfn: A multifunctional wavefunction analyzer. *J. Comput. Chem.* **2012**, *33*, 580−592.

(28) Fuster, F.; Silvi, B. Does the topological approach characterize the hydrogen bond? *Theor. Chem. Acc.* **2000**, *104*, 13−21.

(29) Lyubartsev, A. P.; Laaksonen, A. MdynaMix−A Scalable Portable Parallel MD Simulation Package for Arbitrary Molecular Mixtures. *Comput. Phys. Commun.* **2000**, *128*, 565−589.

(30) Zoete, V.; Cuendet, M. A.; Grosdidier, A.; Michielin, O. SwissParam. A fast force field generation tool for small organic molecules. *J. Comput. Chem.* **2011**, *32*, 2359−2368.

(31) Martínez, L.; Andrade, R.; Birgin, E. G.; Martínez, J. M. Packmol: a package for building initial configurations for molecular dynamics simulations. *J. Comput. Chem.* **2009**, *30*, 2157−2164.

(32) Tuckerman, M.; Berne, B. J.; Martyna, G. J. Reversible multiple time scale molecular dynamics. *J. Chem. Phys.* **1992**, *97*, 1990−2001.

(33) Essmann, U. L.; Perera, M. L.; Berkowitz, T.; Darden, H.; Lee, H.; Pedersen, L. G. A smooth particle mesh ewald method. *J. Chem. Phys.* **1995**, *103*, 8577−8593.

(34) Hoover, W. G. Canonical dynamics: Equilibrium phase-space distributions. *Phys. Rev. A* **1985**, *31*, 1695.

(35) Humphrey, W.; Dalke, A.; Schulten, K. VMD−Visual molecular dynamics. *J. Mol. Graphics* **1996**, *14*, 33−38.

(36) Brehm, M.; Kirchner, B. TRAVIS−A free analyzer and visualizer for Monte Carlo and molecular dynamics trajectories. *J. Chem. Inf. Model.* **2011**, *51*, 2007−2023.

(37) Halappanavar, S.; van der Bruel, S.; Nymark, P.; Gaté, L.; Seidel, C.; Valentino, S.; Zhernovkov, V.; Danielsen, P. H.; de Vizcaya, A.; Wolff, H.; Stoger, T.; Boyadziev, A.; Poulsen, S. S.; Sorli, J. B.; Vogel, U. Adverse outcome pathways as a tool for the design of testing strategies to support the safety assessment of emerging advanced materials at the nanoscale. *Part. Fib. Toxicol.* **2020**, *17*, 16.

(38) Allen, T. E. H.; Goodman, J. M.; Gutsell, S.; Russell, P. J. A History of the Molecular Initiating Event. *Chem. Res. Toxicol.* **2016**, *19*, 2060−2070.
(39) Halappanavar, S.; Sharma, M.; Wallin, H.; Vogel, U.; Sullivan, K.; Clippinger, A. J. *Substance interaction with the lung resident cell membrane components leading to lung fibrosis*. https://aopwiki.org/aops/173 (accessed November 11, 2022).
(40) Marrink, M. A.; Risselada, H. J.; Yefimov, S.; Tieleman, D. P.; de Vries, A. H. The MARTINI force field: coarse grained model for biomolecular simulations. *J. Phys. Chem. B* **2007**, *111*, 7812−7824.
(41) Vazquez-Salazar, L. I.; Selle, M.; de Vries, A. H.; Marrink, S. J.; Souza, P. C. T. Martini coarse-grained models of imidazolium-based ionic liquids: from nanostructural organization to liquid−liquid extraction. *Green Chem.* **2020**, *22*, 7376−7386.
(42) Trott, O.; Olson, A. J. AutoDock Vina: improving the speed and accuracy of docking with a new scoring function, efficient optimization and multithreading. *J. Comput. Chem.* **2010**, *31*, 455−461.
(43) Navia, P.; Troncoso, J.; Romani, L. Excess magnitudes for ionic liquid binary mixtures with a common ion. *J. Chem. Eng. Data* **2017**, *52*, 1369−1374.
(44) Clough, M. T.; Crick, C. R.; Grasvik, J.; Hunt, P. A.; Niedermeyer, H.; Welton, T.; Whitaker, O. R. A physicochemical investigation of ionic liquid mixtures. *Chem. Sci.* **2015**, *6*, 1101−1114.
(45) Chakraborty, M.; Barik, S.; Mahapatra, A.; Sarkar, M. Binary mixtures of ionic liquids: Ideal, non-ideal, or quasi-ideal? *J. Chem. Phys.* **2021**, *154*, 224507.
(46) Gomez, E.; Gonzalez, B.; Calvar, N.; Tojo, E.; Dominguez, A. Physical properties of pure 1-ethyl-3-methylimidazolium ethylsulfate and its binary mixtures with ethanol and water at several temperatures. *J. Chem. Eng. Data* **2006**, *51*, 2096−2102.
(47) Zarei, H.; Keley, V. Density and speed of sound of binary mixtures of ionic liquid 1-ethyl-3-methylimidazolium tetrafluoroborate, N,N-dimethylformamide, and N,N-dimethylacetamide at temperature range of 293.15−343.15 K: Measurement and PC-SAFT modeling. *J. Chem. Eng. Data* **2017**, *62*, 913−923.
(48) Živković, E. M.; Živković, N. V.; Majstorović, D. M.; Stanimirović, A. M.; Kijevčanin, M. L. Volumetric and transport properties of binary liquid mixtures with 1-ethyl-3-methylimidazolium ethyl sulfate as candidate solvents for regenerative flue gas desulfurization processes. *J. Chem. Thermodyn.* **2018**, *119*, 135−154.
(49) Liu, Q.; Ma, L.; Wang, S.; Fu, X.; Wang, J.; Zheng, Q. Study on the properties of density, viscosity, excess molar volume, and viscosity deviation of [C2mim][NTf2], [C2mmim][NTf2], [C4mim][NTf2], and [C4mmim][NTf2] with PC binary mixtures. *J. Mol. Liq.* **2021**, *325*, No. 114573.
(50) Pinto, A. M.; Rodriguez, H.; Colon, Y. J.; Arce, A.; Arce, A.; Soto, A. Absorption of Carbon Dioxide in two binary mixtures of ionic liquids. *Ind. Eng. Chem. Res.* **2013**, *52*, 5975−5984.
(51) Shekaari, H.; Zafarani-Moattar, M. T.; Mokhtarpour, M.; Faraji, S. Compatibility of sustainable solvents ionic liquid, 1-ethyl-3-methylimidazolium ethyl sulfate in some choline chloride based deep eutectic solvents: thermodynamics study. *J. Chem. Thermodyn.* **2020**, *141*, No. 105961.
(52) Anwar, N.; Riyazuddeen; Yasmeen, S. Volumetric, compressibility and viscosity studies of binary mixtures of [EMIM][NTf2] with ethylacetate/methanol at (298.15−323.15) K. *J. Mol. Liq.* **2016**, *224*, 189−200.
(53) Ilokhani, H.; Almasi, M. Densities, viscosities, excess molar volumes, and refractive indices of acetonitrile and 2-alkanols binary mixtures at different temperatures: Experimental results and application of the Prigogine−Flory−Patterson theory. *Thermochim. Acta* **2009**, *495*, 139−148.
(54) Koch, U.; Popelier, P. L. Characterization of C-H-O Hydrogen bonds on the basis of the charge density. *J. Phys. Chem.* **1995**, *99*, 9747−9754.
(55) Luzar, A. Resolving the hydrogen bond dynamics conundrum. *J. Chem. Phys.* **2000**, *113*, 10663−10675.
(56) Yoo, B.; Shah, J. K.; Zhu, Y.; Maginn, E. J. Amphiphilic interactions of ionic liquids with lipid biomembranes: a molecular simulation study. *Soft Matt.* **2014**, *10*, 8641−8651.
(57) Jing, B.; Lan, N.; Qiu, J.; Zhu, Y. Interaction of ionic liquids with a lipid bilayer: a biophysical study of ionic liquid cytotoxicity. *J. Phys. Chem. B* **2016**, *120*, 2781−2789.
(58) Galluzzi, M.; Marfori, L.; Asperti, S.; De Vita, A.; Giannangeli, M.; Caselli, A.; Milani, P.; Podesta, A. Interaction of imidazolium-based ionic liquids with supported phospholipid bilayers as model biomembranes. *Phys. Chem. Chem. Phys.* **2022**, *24*, 27328−27342.

https://doi.org/10.1021/acs.iecr.4c02839
Ind. Eng. Chem. Res. 2025, 64, 1774−1791